

Carbon isotope ratios and nitrogen abundances in relation to cathodoluminescence characteristics for some diamonds from the Kaapvaal Province, S. Africa

B. HARTE¹, I. C. W. FITZSIMONS^{1*}, J. W. HARRIS² AND M. L. OTTER³

¹ Department of Geology and Geophysics, University of Edinburgh, King's Buildings, Edinburgh EH9 3JW, UK

² Division of Earth Sciences, University of Glasgow, Lilybank Gardens, Glasgow G12 8QQ, UK

³ Department of Geological Sciences, University of Cape Town, Rondebosch 7700, South Africa

The colour plates are located at the end of this paper.

ABSTRACT

Secondary ion mass spectrometry (SIMS) techniques have been used to study the variation of C isotope ratio and N abundance within selected diamonds in relation to their crystal growth zones. The growth zones are seen in cathodoluminescence (CL), and include both octahedral and cuboid zones within typical diamonds of external octahedral morphology. Compositions were determined by use of a primary $^{133}\text{Cs}^+$ ion beam and measurement of $^{12}\text{C}^-$, $^{13}\text{C}^-$, and $^{12}\text{C}^{14}\text{N}^-$ secondary ions at high mass resolution on a Cameca ims-4f ion microprobe at Edinburgh University.

In each of the diamonds, different growth zones have marked differences in N abundance, which are as great as 0–1400 ppm within one diamond. Changes of several hundred ppm N are common across both octahedral and cuboid growth zones, and appear sharp and abrupt at the boundaries of the growth zones. In general for the common blue CL, luminescence increases with N abundance. The changes in N abundance across fine scale (~100 μm) growth zones show that the total N contents determined by IR spectroscopy may show great variations of abundance. In contrast, within detection limits, $\delta^{13}\text{C}$ appears constant across many growth zone boundaries. Thus the factors controlling uptake of N from the fluid/melt reservoir in which natural diamonds grow often do not influence $\delta^{13}\text{C}$. No evidence of progressive variation or fractionation of C isotopes during growth was found.

Some original variation in C isotope composition may have been eliminated by diffusion of C atoms subsequent to growth, because of the storage of natural diamonds over millions of years in the Earth's mantle at temperatures of 950–1250°C. Such atomic mobility does not homogenize N distribution because of the proven tendency of N to form aggregates of atoms. A survey of experimental estimates of single atom (C) diffusion parameters, suggests that diffusion distances of ~100 μm are likely at high temperatures (~1100°C) over long time periods (~1.0 Ga). Therefore, with refinement of the diffusion parameters and measurements, the extent of C isotope homogenization in natural diamonds, as well as N aggregation state, might provide quantitative evidence of their time-temperature history under mantle conditions.

KEYWORDS: diamonds, cathodoluminescence, crystal growth zones, nitrogen abundances, carbon isotopes, diffusion.

Introduction

DIAMONDS formed by natural processes not only provide superlative gemstones, but also an exceptional material for many scientific and industrial purposes. The physical properties of

* Present address: School of Applied Geology, Curtin University of Technology, GPO Box U1987, Perth 6001, Australia

diamonds have been determined extensively (e.g. Field, 1992), and their conditions of synthetic growth in the laboratory widely investigated (e.g. Burns and Davies, 1992; Sato and Kamo, 1992; Kanda, 1996). From the Earth Science viewpoint, natural diamonds have been the subject of extensive research because they provide information on mantle geochemistry, mineralogy and pressure-temperature regimes. These data are derived both by investigation of the diamonds themselves, for C, N and growth attributes, but also from studies of inclusions of other minerals in diamonds (e.g. Robinson, 1978; Deines, 1980, 1996; Harris, 1987, 1992; Meyer, 1987; Gurney, 1989). Whilst the broad pattern of igneous, metamorphic and geophysical behaviour in the mantle must control both silicate mineral genesis and diamond formation (e.g. Javoy *et al.*, 1986; Galimov, 1991; Haggerty, 1986), it is possible that the detailed physico-chemical circumstances controlling diamond crystallization may not be closely linked in time to some circumstances controlling silicate mineral development (Deines, 1996). Thus diamond crystallization must be closely linked to element abundances and thermodynamic conditions within the C-O-H-N system, but is perhaps relatively little affected by heavier element abundances and geochemistry involving the silicate minerals. On the other hand, it must always be the case that the abundance and oxygen fugacity of C-O-H-N fluids have a major effect on silicate mineralogy and melting as well as diamond crystallization (Haggerty, 1986; Taylor and Green, 1989; Galimov, 1991).

This contribution is concerned with the application of ion microprobe techniques to examining the relationships between three major features of natural diamonds: (1) detailed crystal growth history, which is usually excellently displayed by cathodoluminescence (CL); (2) C isotope compositions; and (3) variations in N abundance. The ion microprobe allows C and N analysis on the scale of microns and therefore the measurement of geochemical characteristics associated with individual growth zones of diamonds.

As the only major element compositional variable of diamonds, relative C isotope abundance has been widely documented with a view to distinguishing different mantle provenances (e.g. Javoy *et al.*, 1986; Deines *et al.*, 1991; Galimov, 1991), different isotope fractionation characteristics (e.g. Deines, 1980; Boyd *et al.*, 1994), and potential crustal progenitors (e.g. Kirkley *et al.*,

1991). Nitrogen abundance, distribution, and state of aggregation in the diamond crystal lattice have been investigated widely in both natural and synthetic diamonds, because it is the principal impurity of diamonds and therefore has a marked effect on its electrical, optical and mechanical properties (e.g. Chrenko *et al.*, 1977; Evans, 1992; Lang *et al.*, 1992; Stoneham, 1992). Furthermore, the extent of aggregation of N has been used as an indicator of time-temperature history for natural diamonds (e.g. Evans and Harris, 1989; Taylor *et al.*, 1996; Richardson and Harris, 1997).

Until recently, C isotope determinations have been carried out by combustion of diamond and analysis by gas source mass spectrometry. Some studies of individual parts of diamond crystals have been conducted by laser cutting of diamonds, and major discontinuities in diamond growth, such as those of 'coated' stones, have been investigated in this way (e.g. Swart *et al.*, 1983; Boyd *et al.*, 1992). Nitrogen element abundances may also be determined by combustion techniques, but more usually both N abundance and aggregation state are determined by Fourier Transform infrared (FTIR) spectrometry (Evans, 1992; Taylor *et al.*, 1996). In this case the surface area targeted by the IR beam may be as small as 20 μm in diameter, but the method is a transmission technique and thus the volume actually sampled is dependent on the thickness of the diamond plate under investigation. By using ion microprobe techniques, we are able to present quantitative variations in both C isotope composition and N abundance for surface sample areas on the scale of 5–10 μm and with sampling depths of <5 μm . Thus it has been possible to monitor both C isotope composition and N abundance for individual fine scale crystal growth zones.

The detailed ion microprobe studies presented here have focused on a small number of diamonds from the well known Kaapvaal craton province of South Africa. They were selected for investigation because they had evident and interesting growth zonation features when examined by CL, but no evident zonation or discontinuities when viewed through an ordinary binocular light microscope. As far as we are aware they are typical of many of the natural diamonds recovered for gem production. Detailed studies of both C isotopes and N have focused on three diamonds and are reported in detail here. Two of these diamonds (J/1064.2 and J/1063.1) are from the Bultfontein mine and form part of a selection of diamonds studied by Wilding (1990) and Wilding *et al.* (1994); the

third diamond (specimen K3) is from Koffiefontein. In addition, preliminary C isotope studies have been made on three other Kaapvaal diamonds, one from Finsch and two (one of peridotitic and the other of eclogitic paragenesis) from Premier. These Finsch and Premier diamonds show similarities to the Bultfontein stones described here, in that their variation in C isotope composition is restricted, despite showing conspicuous growth zones in CL. The three diamonds studied in detail for both C isotopes and N showed no inclusions to indicate a paragenesis. Previous studies have shown the Bultfontein and Koffiefontein diamonds to be largely of peridotitic rather than eclogitic paragenesis (Wilding *et al.*, 1994; Harris and Gurney, 1979); but the alternating cuboid and octahedral growth zones shown for J/1064.2 are perhaps more characteristic of eclogitic than peridotitic diamonds (Bulanova, 1995). The nicknames ('wild-one' and 'whopper') are commonly used to refer to the stones J/1064.2 and J/1063.1 from Bultfontein respectively.

All three diamonds, at least in their outer parts, show the extensive development of flat octahedral faces typical of most natural diamonds (Harris *et al.*, 1975), and associated with growth from a melt/solution (Sunagawa, 1984). The CL characteristics of the polished surfaces of the diamonds are shown in the coloured images of Plates 1 and 2. The FTIR studies have been possible on Bultfontein diamond J/1064.2 ('wild-one'), which has been cut to a thin plate, and have shown IaA to IaB N aggregation characteristics similar to much of Kaapvaal diamond production

(Evans and Harris, 1989; Deines *et al.*, 1991, 1993; Wilding *et al.*, 1994). The pieces of diamonds J/1063.1 ('whopper') and K3 studied are too thick or irregular for satisfactory FTIR investigation. Since the relationships between growth history as seen in CL, and the spatial variation of N and C isotope characteristics, form an important aspect of this study, we describe the features seen in CL (Plates 1 and 2) in conjunction with presentation of the geochemical data in the results section of the paper.

Methods

Nitrogen abundance and C isotope composition in natural stones and synthetic standards were measured using a CAMECA ims-4f ion microprobe (Slodzian, 1980), with a Charles Evans & Associates control system for magnetic peak switching, at the NERC Facility in the Department of Geology and Geophysics, University of Edinburgh. The principal operating conditions are summarized in Table 1. Given the limited use to date of SIMS in determining C isotope ratios ($\delta^{13}\text{C}$) and N abundance (N_{ppm}) in diamonds, we give a relatively full account here of the procedures followed for sample preparation, analysis, and data reduction in these studies.

Sample preparation and standardization

The natural diamonds were cut and polished parallel to $\{100\}$, and examined and photographed in cathodoluminescence (CL) to show evidence of growth structure and history. For ion

TABLE 1. Summary of ion microprobe operating conditions

	C isotopes	Nitrogen
Primary beam ions	$^{133}\text{Cs}^+$	$^{133}\text{Cs}^+$
Primary beam net potential	+14.5 kV	+14.5 kV
Primary beam current	0.3 nA or 0.5 nA	5.5–8 nA
Primary beam spot size	5 μm or 40 μm	~20 μm
Diameter of area sampled	~5 μm or ~8 μm	~8 μm
Secondary extraction potential	-4.5 kV	-4.5 kV
Energy window	25–50 eV	10–25 eV
Secondary ions	$^{13}\text{C}^-$ and $^{12}\text{C}^-$	$^{14}\text{N}^{12}\text{C}^-$ and $^{13}\text{C}^-$
Counting	5 s $^{13}\text{C}^-$, 1 s $^{12}\text{C}^-$ for 100 cycles	2 s $^{14}\text{N}^{12}\text{C}^-$, 2 s $^{13}\text{C}^-$ for 50 cycles
Mass resolution (m/ Δm)	~4300	~7500
Usual error at ± 1 s level	0.6 to 0.9%	3–5%

microprobe analysis the samples and standards were pressed into indium to give a smooth flat surface, and then the mount was washed with acetone in an ultrasonic bath and coated with a thin layer of gold ($\sim 0.02 \mu\text{m}$). Lines of silver DAG were painted on the surface to further ensure conductivity between the diamonds and the sample holder.

All measurements for $\delta^{13}\text{C}$ and N_{ppm} were referenced to synthetic diamond standards supplied by the Diamond Trading Company (Maidenhead). Nearly all the data reported here were gathered in the period 1990 to 1992 and referenced to the first diamond standard (referred to as 'oldstandard') made available to the Edinburgh Laboratory. The isotopic composition ($\delta^{13}\text{C}_{\text{PDB}}\text{‰}$) of this standard has been determined as $-23.33 \pm 0.03\text{‰}$ (all uncertainties in this paper are given as ± 1 standard deviation, $\pm s$), on the basis of bulk combustion of another part of the same synthetic diamond (analysis done by M.C. Wilding at Scottish Universities Research and Reactor Centre, see Wilding, 1990), and repeated SIMS analysis of the 'oldstandard' relative to a second synthetic diamond standard ('synthetic A'), which was used extensively by Fitzsimons *et al.* (1999) in a companion study of diamonds from Colorado. In a preliminary discussion of C isotope variation in the Koffiefontein K3 stone, Harte and Otter (1992) adopted a slightly erroneous C isotope composition for the 'oldstandard', and in the present paper all the K3 data are re-calibrated with the correct standard composition.

Several other synthetic diamonds were examined by ion microprobe in these studies, and these also showed considerable homogeneity in $\delta^{13}\text{C}$ to within $\pm 1\text{‰}$ but were found to have variation in N abundance related to growth layers and sectors as described by Burns *et al.* (1990). The N standard for ion microprobe analysis was chosen as a slice taken from one of these synthetic diamonds, called the 'synthetic A' standard. This slice showed homogeneous N concentration on the ion microprobe; and an adjacent piece of the same homogeneous region was determined as having $230.4 N_{\text{ppm(wt)}}$ and $\delta^{13}\text{C}_{\text{PDB}}$ of -23.924‰ by combustion analysis (analyses by S.R. Boyd, at the Laboratoire de Géochimie des Isotopes Stables, Université de Paris VII). The N content of 'oldstandard' was found to be homogeneous and determined as $77.8 \pm 1.5 \text{ ppm}$ by repeated SIMS analysis relative to the 'synthetic A' standard.

Carbon isotope analysis

Carbon forms negative ions readily and SIMS is an effective means of C isotope measurement (e.g. McKeegan *et al.*, 1985; Zinner *et al.*, 1989). A primary beam of $^{133}\text{Cs}^+$ ions, which enhances the secondary ion yield of electronegative elements (Storms *et al.*, 1977), was used to sputter secondary ions from the sample, and count rates of $^{12}\text{C}^-$ and $^{13}\text{C}^-$ ions were used to determine the isotope composition by comparison with counts from a standard of known $\delta^{13}\text{C}$. The use of a positive primary beam and extraction of negative secondary ions causes a positive charge build-up on the surface of insulating samples, which has a significant effect on the yield of secondary ions. However, it appears that diamond is conductive enough to dissipate charge (Harte and Otter, 1992), and, as in other SIMS studies of relatively conducting minerals (e.g. oxygen isotopes in magnetite; Valley *et al.*, 1998), we were able to perform multiple analyses across a large sample area with no evidence of sample charging.

The data from the first analytical session (December 1990, sample K3) reported here were collected with a focused primary Cs^+ beam ($\sim 5 \mu\text{m}$ pit diameter on the sample) and a beam current of $\sim 0.3 \text{ nA}$, but the remainder of the C isotope analyses were performed with a defocused primary beam ($\sim 40 \mu\text{m}$) and a beam current of $\sim 0.5 \text{ nA}$. The use of the defocused beam reduces the progressive isotope fractionation that can occur in the relatively deep but narrow pits produced by a focused primary beam. In both cases the primary beam was accelerated at a net potential of $+14.5 \text{ kV}$ onto the sample, and the sputtered negative secondary ions were accelerated at a potential of -4.5 kV towards the electrostatic energy filter and mass analyser. The contrast diaphragm was set at $150 \mu\text{m}$. A large field aperture ($1800 \mu\text{m}$) was used for those analyses made with a focused primary beam, but a small field aperture ($100 \mu\text{m}$) was selected for secondary ions generated by a defocused beam so that only those ions from the central $8 \mu\text{m}$ of the sputtered area were admitted to the energy filter. As well as keeping the analysed area small, this also reduces the counts to acceptable values. The settings for the energy window (Table 1) depended on mass resolution, but were usually 50 eV for C isotopes.

In SIMS analysis of $^{12}\text{C}^-$ and $^{13}\text{C}^-$ the principal mass interference is that of the $^{12}\text{CH}^-$ hydride with the $^{13}\text{C}^-$ ions. In analysis, the

entrance and exit slits were adjusted to achieve a mass resolution of ~ 4300 ($m/\Delta m$, where Δm is the mass separation between two species with average mass m), which gave a clear separation of the $^{12}\text{CH}^-$ and $^{13}\text{C}^-$ peaks. The degree of hydride interference was also minimized by maintaining a high vacuum in the sample chamber ($< 2 \times 10^{-9}$ Torr). Secondary ions in the first two major C sessions (December, 1990; July, 1991) were measured using Balzers SEV217 electron multipliers of various ages (Harte and Otter, 1992). The final session of C analysis (1992) used an ETP AF133 electron multiplier, which was installed at the start of the session.

Nitrogen analysis

The SIMS analysis of N is problematic because N does not readily form positive or negative secondary ions (Storms *et al.*, 1977). However in the presence of C, N does form secondary CN^- ions, and this has been used as a SIMS monitor of trace N in carbonaceous materials such as SiC and graphite (Zinner *et al.*, 1989; Hoppe *et al.*, 1995). Secondary $^{12}\text{C}^{14}\text{N}^-$ ions were measured relative to $^{13}\text{C}^-$ ions in the diamond samples and referenced to similar measurements on the diamond standards. Operating conditions for N analysis were largely similar to those used for determination of C isotopes, but with a higher primary beam current and using a narrower energy window to achieve higher mass resolution (Table 1). Calculated errors for N analyses are small ($< 5\%$) compared with the wide variations in N_{ppm} seen in the diamonds, and abundances of < 5 ppm may be detected.

Analytical procedure

Following a burn-in time of 5 min, required to remove the gold coat and allow the sputtering process to achieve a steady state, the negative secondary beam ions were detected with the electron multiplier. Each C isotope analysis comprised 100 measurement pairs (100 cycles), with each cycle consisting of a 1 s count time for ^{12}C and a 5 s count time for ^{13}C . A N analysis comprised either 30, or more usually 50, measurement pairs (50 cycles), with each cycle involving a 2 s counting period for both $^{12}\text{C}^{14}\text{N}$ and ^{13}C . The primary beam current was checked before and after each analysis and adjusted if there was significant drift. The position of the primary beam spot was also imaged at the start

and end of each analysis, in order to check the primary beam position and centralization of both the secondary beam and the field aperture. In addition, the magnet was re-calibrated before each analysis, during the burn-in time.

The synthetic standard was analysed at regular intervals during each session, typically after every 3–5 sample analyses in the case of C, but less frequently for the N analyses (Fig. 1). Such close monitoring of the standard is essential for the C isotope measurements in order to keep a close check on errors and monitor drift in $^{13}\text{C}/^{12}\text{C}$ ratio during the course of an analytical session (see below). In the first N analytical session (July 1991 on 'wild-one') N was determined relative to ^{13}C but no standards were analysed, and the relative N concentrations obtained during this session have been calibrated by reference to other measurements made on the same stone during a later session (January 1992) for which standard data are available.

Since the growth zone features of the diamonds are only visible in CL (Plates 1 and 2), the exact location of analysis pits with respect to the growth zones were determined from CL photographs of the diamond plates taken after each analytical session.

Data reduction

The count data for all sample and standard analyses were expressed as $^{13}\text{C}/^{12}\text{C}$ and $^{12}\text{C}^{14}\text{N}/^{13}\text{C}$ ratios for each measurement pair, and then corrected for the counting system dead time, which was determined for each analytical session by making a series of measurements at varying count rates. Any errors arising from dead-time correction were minimized by having similar count rates for the major ^{12}C ion on samples and standard; these being set at 5×10^5 counts per second at the start of each session, and kept at this value by regular checks and adjustments of the primary beam current.

In each point measurement of 100 or 50 cycles, the abundance ratio from each cycle nearly always fell inside three times the standard deviation (± 3 s) of the mean ratio value. Occasional cycle ratios which fell outside ± 3 s were rejected and the remaining data were then used to calculate a final mean value of either $^{13}\text{C}/^{12}\text{C}$ or $^{12}\text{C}^{14}\text{N}/^{13}\text{C}$ for each analysis point. The uncertainty associated with each mean ratio was calculated as a standard error of the mean, and in all cases this closely matches the precision

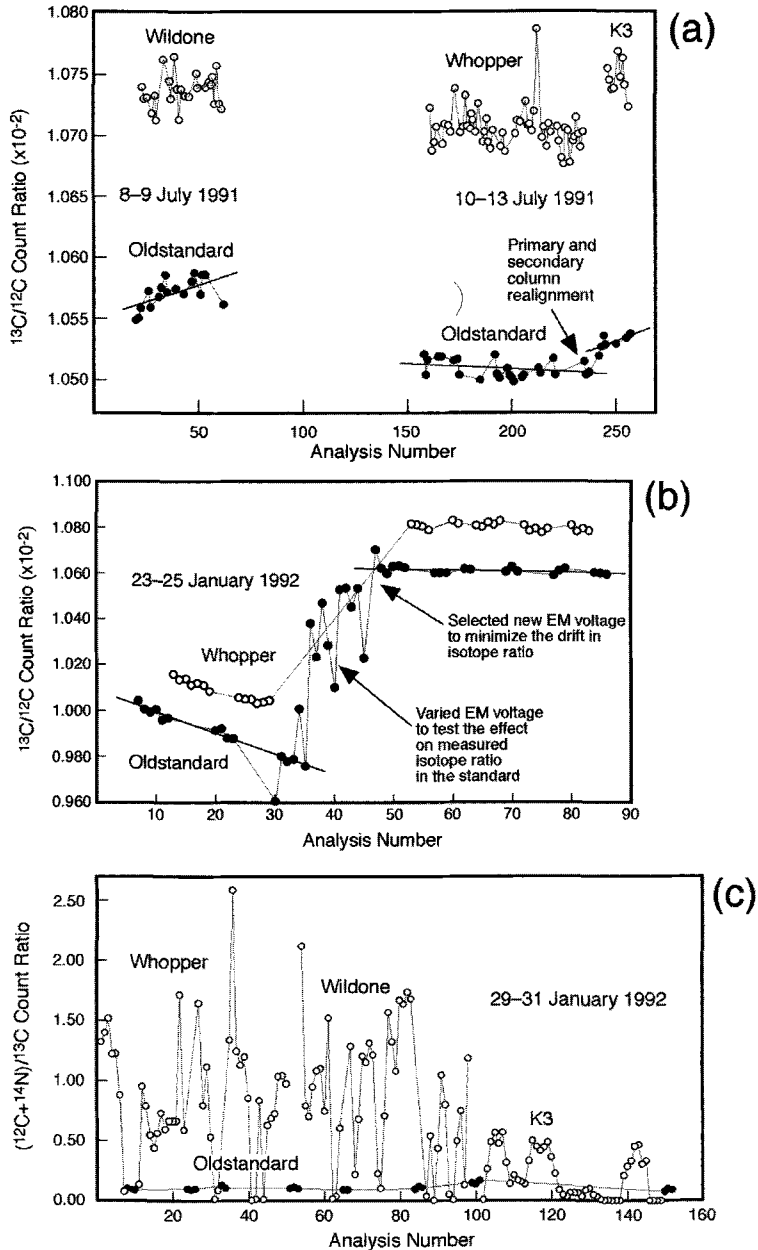


FIG. 1. Variations in ion ratios measured for samples and standards during main periods of analysis: (a) C isotope data of July, 1991; (b) C isotope data of January, 1992; (c) N data of January, 1992. Data for particular samples (as named) are shown as open circles; standard data ('oldstandard') are solid circles. Each point represents the average of either 100 ratio measurements (cycles) of ion ^{13}C and ion ^{12}C , or 50 ratio measurements (cycles) of 'molecule' ($^{12}\text{C}+^{14}\text{N}$) and ion ^{13}C . Regression lines, indicating the drift in average standard values during the course of analysis, are also shown. Drift in the standard values may be seen to be reasonably linear, except where adjustments were made to the instrument. Errors calculated in the Tables (2-7) take account of both the standard deviation of the 100 or 50 cycles of each point and the calibration against the standard (see text and Fitzsimons *et al.*, 2000).

predicted by Poisson counting statistics (see Fitzsimons *et al.*, 1999b). The variations in these mean ratios for standard and sample analyses during the main analytical sessions, excluding the earliest sessions are depicted in Fig. 1; a similar diagram for the earliest C isotope sessions on diamond K3 was presented by Harte and Otter (1992). It is immediately apparent that whereas the variations in $^{12}\text{C}^{14}\text{N}/^{13}\text{C}$ ratio are far greater in the natural diamond plates than in the synthetic standard, variations in $^{13}\text{C}/^{12}\text{C}$ ratio may be rather similar in both sample and standard material.

The measurement of the standards is essential to correct for fractionation of the natural ion abundances during analysis. Data reduction must allow for variation in this fractionation due to drift in instrument response over analytical sessions lasting hours or even days. This is a common problem in SIMS analyses of this type (Slodzian *et al.*, 1997), and drift in the $^{13}\text{C}/^{12}\text{C}$ ratio is obvious from the standard data illustrated in Fig. 1. Each analytical session can be divided into a number of sections with a fairly consistent drift, and the breaks between these sections invariably correspond to significant changes in the instrumental set up (Fig. 1). Least-squares regression lines were calculated for standard data in each of these consistent sections, and then used to calculate $\delta^{13}\text{C}$ values for the sample data, thus correcting for the effects of mass fractionation and for the gradual drift in measured isotope ratios (Fitzsimons *et al.*, 2000). In most cases, the drift involves a steady decrease in $^{13}\text{C}/^{12}\text{C}$, which has been interpreted in terms of electron multiplier ageing (e.g. Eiler *et al.*, 1995). Drift in the reverse sense is also observed, typically immediately after instrument start-up or major realignment, and presumably represents an instrumental response to changes in the primary and/or secondary column. Regression lines were also calculated for the N standard data, although the magnitude of any drift in this case is relatively insignificant (Fig. 1) compared to the variations in N abundance in the natural stones.

Uncertainties are given in data tables for isotope ratios and for $\delta^{13}\text{C}$ values or N concentrations (± 1 s in all cases), and were calculated using the statistical relationships discussed by Fitzsimons *et al.* (2000). In the case of the C isotope data the permil differences in isotope ratio are small and errors have to be considered carefully in assessing variations between the growth zones of each diamond

plate. Therefore, in Tables 3, 5 and 7, in addition to the $\delta^{13}\text{C}$ values calculated by calibration against the standard regression lines, we list for each (100 cycle) analysis point the mean values of $^{13}\text{C}/^{12}\text{C}$ and their standard errors of the mean (equivalent to the relative standard deviation of the total accumulated counts for the 100 cycles). This allows comparison of the error of a 100 cycle single point analysis with the overall permil error, which also includes referencing the single analysis to the standard and taking account of the drift of standard values discussed above. In permil terms the overall uncertainty (± 1 s) determined for a $\delta^{13}\text{C}$ value is usually very close to that found for the $^{13}\text{C}/^{12}\text{C}$ ratio (Tables 3, 5 and 7). We take this as evidence that the standard was measured sufficiently frequently to allow compensation for instrumental variation over time during the analysis sessions.

In comparing the data for various growth zones, we have made use of 'two sample *t* tests' for comparing mean compositions. All calculations have been done using the 'Minitab' computer package, calculating '*t*' and '*p*' and using a 95% confidence interval (Ryan and Joiner, 1994).

Results

Bultfontein specimen J/1064.2 ('wild-one')

CL Zones

Plate 1 shows the CL zones as seen in the analysed thin plate cut approximately across the centre of this diamond. In the extensive development of octahedral (flat) and cuboid (rounded-hummocky) surfaces, the growth structure of this diamond shows marked similarities to that of specimen 535A described in detail by Lang (1974a). For the convenience of description the growth zones have been separated into major sets of zones (A, B, C, D, E) according to major discontinuities in the growth structure, and these major zones are further divided into subzones (Fig. 2a) according to the colour and intensity of CL. Compared to Lang's 535A specimen, the inner centre-cross structure is not marked by large differences in luminescence (Plate 1), but we clearly portray its shape in Fig. 2a. Subzones (B1–B3) with cuboid growth laminae, surround the centre cross, and are sharply bounded outwards by an extensive octahedral surface. As with zone B, the major and minor internal growth structures of zones C and D (Plate 1 and Fig. 2a) are dominated by cuboid shapes, but with extensive octahedral outer bounding surfaces. In

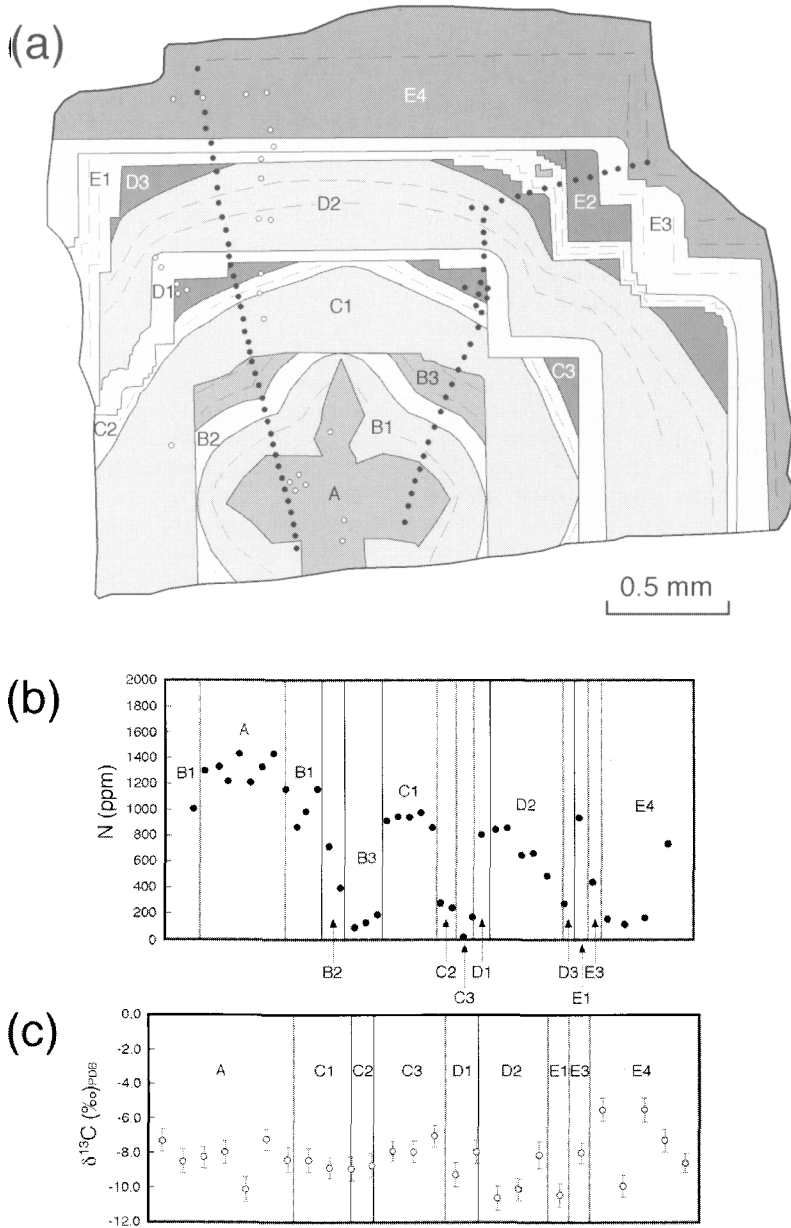


FIG. 2. CL zones with N_{ppm} and $\delta^{13}\text{C}\text{‰}$ for the 'wild-one' diamond (see also Plate 1). (a) Summary of the major sets of zones (A, B, etc.) and subzones (B1, B2, etc.) as seen in CL, together with the positions of ion microprobe analysis points (solid dots being for N abundance and open circles for C isotope ratio) corresponding with data given in Figs 2b and 2c and Tables 2 and 3. Note that the very dark zones, following outwards from C2, D2 and E1 are C3, D3, and E2, respectively, and correspond to the greenish-yellow or very dark blue zones in Plate 1. Fig. 2(b) and (c) show N_{ppm} , (by weight) and $\delta^{13}\text{C}\text{‰}$ respectively, for the analysis points of the left hand transect of Fig. 2a. Error bars, as standard errors of the mean and equivalent to ± 1 s deviation (Fitzsimons *et al.*, 2000) are given for the C isotope ratio. Errors for the N are often smaller than the symbol (see Table 2 for compilation) and are not shown.

the outermost part of the diamond, the E zones form a shell of largely octahedral habit. Some short segments of the E zone boundaries do have a cuboid orientation, although this may be seen (e.g. particularly in subzone E1 in the upper left of Plate 1 and Fig. 2a) to be largely a result of the repetition of small octahedral faces in two directions at right angles. Other boundaries in the C and D parts of this diamond also suggest that the very small scale repetition of growth on two octahedral faces may give the appearance of growth on hummocky surfaces of mean cuboid orientation. This possible mode of development of cuboid surfaces has also been noted by Lang (1974a), and appears to contrast with cuboid growth involving a fibrous or columnar habit (Lang, 1974b; Sunagawa, 1984).

N and $\delta^{13}\text{C}$ data

Figure 2a shows solid points marking the positions of N analyses along two transects across the diamond plate, and open circle points showing C isotope analytical positions in the region adjacent to the left-hand N transect. On Plate 1 the points of N and C analysis are not visible since the analyses were made on the opposite side of the diamond plate. Tables 2 and 3 list the quantitative results of all the analyses commencing with analysis points at the bottom of Fig. 2a for each transect. The N_{ppm} and $\delta^{13}\text{C}_{\text{PDB}}\%$ results for the left-hand transect (or 'transect one' of Table 2) are also shown graphically with respect to position within the CL zones in Figs 2b and 2c. It may be seen from Table 2 that the N abundance pattern with respect to CL zones is very similar for both transects of the diamond.

Comparison of Figs 2a and 2b and Plate 1 shows that there is a very close correlation between brightness and zonation in CL and N abundance. The brighter and paler blue zones of Plate 1 (e.g. A, B1, C1) all show N abundances approaching 1000 ppm or above, whilst N abundance drops in the subzones of darker and deeper blue colours. This is seen well in the progressive changes across each of the B, C and D sets of subzones, which culminate in very dark blue or yellow-green CL colours (e.g. B3, C3, D3) characterized by <50 ppm N.

In contrast to the conspicuous variations in N abundance, the $\delta^{13}\text{C}$ values for the 'wild-one' diamond show restricted variation. The data (Table 3 and Fig. 2c) fall mostly within 2 s of a normal or Gaussian distribution with a mean of

$-8.35 \delta^{13}\text{C}\%$. No pattern of variation or correlation with CL is evident, in contrast to the N data.

A check with FTIR microspectroscopic techniques for N abundance and aggregation states was carried out on the 'wild-one' plate at the Diamond Trading Centre (Maidenhead). Determinations by FTIR were made in the centre of zones A, B3, C1, C2, C3, D2, E2, and E4, as seen in Fig. 2a. All showed type Ia aggregation states; with the IaA/(IaA+IaB) ratio being 64 to 78%, except in subzones E2 and E4 where it is recorded as 87 and 98% respectively. The N_{ppm} estimated by FTIR for the central parts of the subzones A, B3, C1, C2, C3, D2, E2, and E4, respectively are: 1381, 706, 1091, 524, 438, 760, 176, and 247. These values show reasonable agreement with the ion microprobe data (Table 2, Fig. 2b) for the broader and more homogenous zones (A, C1, D2, E4), but poorer agreement with the narrower and more complex zones (B3, C2, C3, E2). This may be explained by the fact that the FTIR transmission technique, will have sampled several growth subzones in the case of the narrow more complex zones, because of the changes in detailed structure as seen on the two sides of the 'wild-one' plate (Plate 1, Fig. 2a).

Bultfontein specimen J/1063.1 ('whopper')

CL zones

Plate 2a shows a complex growth history, dominated by cuboid growth in the more internal parts of the diamond and by octahedral growth in more external parts. The dominantly cuboid growth region shows wide and narrow zones, which are broadly concentric but cross-cut one another locally. As with the 'wild-one' such cross-cutting is most conspicuous (e.g. in the lower left quadrant of the diamond) where a change from cuboid to octahedral orientations takes place. In the outer part of the diamond, regular, parallel and often thin octahedral zones are well developed.

N and $\delta^{13}\text{C}$ data

Figure 3a shows the position of the measured points in the 'whopper' together with the principal features of growth zones, which are divided into sets (A, B, C, D) and subsets (A1, A2 etc.) according to the major changes and discontinuities of growth pattern. Most ion microprobe measurements have been made in an upper left to lower right transect across the diamond (Fig. 3a,

TABLE 2. N abundance data on Bultfontein diamond J/1064.2 ('wild-one')

CL zone	Analysis point*	N content (wt. ppm)	1 s (\pm) (wt. ppm)**	N content (atomic ppm)
Transect one (left side of Fig. 2a)				
B1	1	1004	n/a	861
A	2	1299	n/a	1114
A	3	1331	n/a	1141
A	4	1218	n/a	1045
A	5	1430	n/a	1226
A	6	1207	n/a	1035
A	7	1326	n/a	1137
A	8	1430	n/a	1226
A/B1	9	1156	n/a	991
B1	10	865	n/a	742
B1	11	982	n/a	842
B1	12	1157	n/a	992
B2	13	715	n/a	614
B2	14	392	n/a	336
B3	15	90	n/a	77
B3	16	129	n/a	111
B3	17	191	n/a	163
C1	18	912	n/a	782
C1	19	945	n/a	810
C1	20	944	n/a	810
C1	21	979	n/a	839
C1	22	861	n/a	738
C2	23	279	n/a	239
C2	24	240	n/a	206
C3	25	19	n/a	16
C3/D1	26	171	n/a	146
D1	27	805	n/a	690
D2	28	847	n/a	726
D2	29	859	n/a	737
D2	30	648	n/a	555
D2	31	666	n/a	571
D2	32	487	n/a	418
D2/D3	33	279	n/a	239
E1	34	938	n/a	805
E3	35	443	n/a	380
E4	36	162	n/a	139
E4	37	120	n/a	103
E4	38	171	n/a	147
E4	39	740	n/a	635

Transect two (right side of Fig. 2a)

A	1	1636	54	1403
A	28	1259	63	1080
A	27	1309	65	1122
A	26	1231	60	1056
A	25	1254	60	1075
B1	24	814	38	698
B1	23	998	46	856
B1	22	1185	54	1016
B2	21	534	24	458
B3	20	81	3	69

TABLE 2. (contd.)

CL zone	Analysis point*	N content (wt ppm)	1 s (\pm) (wt ppm)**	N content (atomic ppm)
B3	19	171	7	147
C1	18	920	38	789
C1	17	998	42	856
C1	16	877	36	752
C1	15	917	36	787
C2	14	515	20	442
C2	11	461	16	395
C3	10	29	1	25
C3	29	27	1	23
C3	9	12	0	11
C3/D1	13	167	7	143
C3/D1	12	983	38	843
D1	8	1167	40	1001
D1	7	577	20	495
D2	6	849	29	728
D2	5	835	27	716
D2	4	733	24	629
D2	2	615	19	527
D2	3	544	17	466
D2	30	362	17	311
D3	31	0	0	0
D3/E1	32	277	11	238
E1	33	653	25	560
E1	34	486	18	417
E2	35	33	1	28
E2	36	2	0	2
E3	37	282	10	242
E3	38	417	15	357
E4	39	70	2	60
E4	40	634	26	544

* Analysis points are numbered according to their order of collection for each transect; but they are listed in the order of their distribution along each transect starting at the bottom of the diamond as seen in Fig. 2a.

** Errors are standard errors of the mean for measurements (50 cycles) made on each point and taking into account variation in the standard value during a continuous analytical session; they do not include error in the absolute value of the standard as determined by combustion. No errors are given for transect 1, because the standard was not measured during the course of the point analysis.

and Tables 4 and 5), with several shorter traverses of similar orientation being made in the lower right area to check the consistency or variability of data from the region of finely spaced octahedral growth zones.

All the N_{ppm} and $\delta^{13}C_{PDB}\%$ data for the 'whopper' are given in Tables 4 and 5, and are

CATHODOLUMINESCENCE CHARACTERISTICS

TABLE 3. C isotope data for Bultfontein diamond J/1064.2 ('wild-one')

CL zone	Analysis point*	$^{13}\text{C}/^{12}\text{C} \times 10^{-2}$		$\delta^{13}\text{C}$	
		value	1 σ (\pm)**	‰PDB	1 σ (\pm)***
A	17	1.075	0.0007	-7.32	0.69
A	19	1.074	0.0007	-8.54	0.74
A	20	1.074	0.0006	-8.28	0.69
A	22	1.075	0.0006	-8.00	0.74
A	25	1.073	0.0007	-10.13	0.84
A	24	1.076	0.0006	-7.27	0.74
A	18	1.074	0.0007	-8.45	0.76
C1	21	1.074	0.0007	-8.45	0.78
C1	16	1.073	0.0006	-8.90	0.63
C2	15	1.073	0.0007	-8.94	0.72
C2/C3	14	1.073	0.0007	-8.74	0.69
C3	3	1.073	0.0006	-7.93	0.64
C3	2	1.073	0.0006	-7.96	0.68
C3	1	1.074	0.0006	-7.02	0.69
D1	4	1.072	0.0007	-9.28	0.73
D1	5	1.073	0.0007	-7.95	0.69
D2	26	1.072	0.0007	-10.62	0.81
D2	23	1.073	0.0006	-10.08	0.74
D2	13	1.074	0.0008	-8.13	0.76
E1	12	1.071	0.0007	-10.43	0.68
E3	11	1.074	0.0006	-8.00	0.59
E4	10	1.076	0.0007	-5.49	0.65
E4	6	1.071	0.0006	-9.88	0.63
E4	7	1.076	0.0007	-5.45	0.71
E4	8	1.074	0.0006	-7.24	0.62
E4	9	1.073	0.0006	-8.56	0.56

* as for Table 2; points on Fig. 2a.

** standard error of the mean for 100 cycles measured on point.

*** ‰ error including error of $^{13}\text{C}/^{12}\text{C}$ point measurement and error of repeated standard analysis during continuous period of ion microprobe analysis.

illustrated in Figs 3b and 3c. As with the 'wild-one' diamond, N abundance shows a correlation with the CL, with the more luminescent and paler blue growth zones (e.g. A1, A2, C1) showing higher N contents; whilst the very dark, virtually non-luminescent, zone B shows <10 ppm N in all transects (Table 4). This correlation also applies to the finely alternating octahedral growth zones in the lower right region of the main transect, with the exception of one low luminescent narrow zone which gave a high N_{ppm} of 1367. The reason for this singular exception is unknown; a mass scan on the ion microprobe showed no clear evidence of other elements besides C and N.

The $\delta^{13}\text{C}$ data (Fig. 3c) for the 'whopper' show a relatively small range of values, and there is little sign of correlation with either CL zones or N_{ppm} . In Fig. 4a the whole of the $\delta^{13}\text{C}$ data are

shown in a frequency vs composition plot. Statistical comparisons of different zones and subzones of the 'whopper' were made using two-sample t tests (Ryan and Joiner, 1994) with 95% confidence limits. These indicate that despite the overall small range of compositions, there is a definite difference between the mean $\delta^{13}\text{C}$ values for zones A and D (with $t = -3.94$ and $p = 0.0003$). However, the $\delta^{13}\text{C}$ data from the dominantly cuboidal zone C is not statistically separable from that for the octahedral zone D ($t = -0.09$, $p = 0.93$). Although its dataset is limited for statistical analysis, the narrow zone B (very low N_{ppm} and black in CL, Plate 2a) is intermediate in mean composition between A and C+D.

Figures 4b and 4c give details for the region in the bottom right (Fig. 3a) of the 'whopper', where

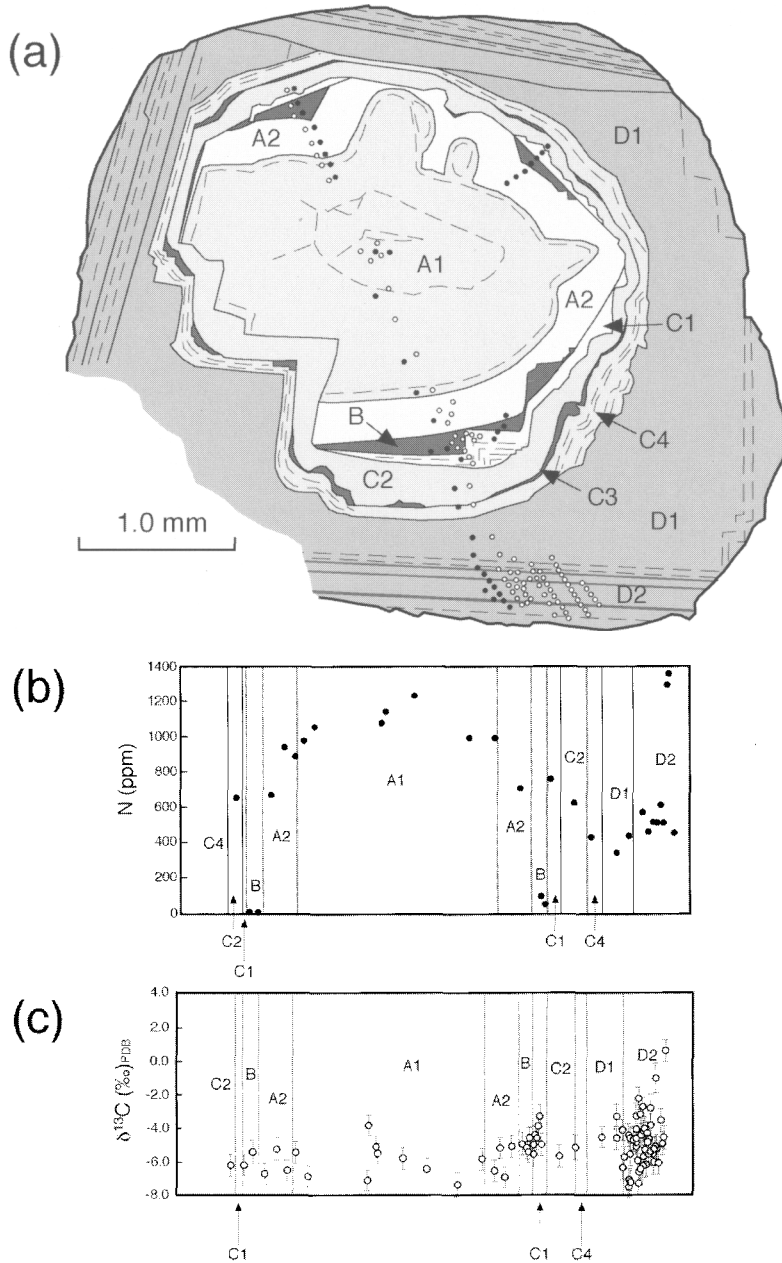


FIG. 3. CL zones with N and $\delta^{13}\text{C}$ ‰ for the 'whopper' diamond (see also Plate 2a). (a) Summary of major sets of CL zones (A, B, etc) and subzones (e.g. A1, A2) together with positions of ion microprobe analysis points (solid dots being for N abundance and open circles for C isotope ratio) corresponding with data given in Figs 3b and 3c and Tables 4 and 5. Note that zone B with very low N_{ppm} corresponds to the discontinuous very dark (black) zone in Plate 2a. (b) and (c) show N_{ppm} (by weight) and $\delta^{13}\text{C}$ ‰ respectively, for the analysis points along the transect running from top left to bottom right of Fig. 3a. Error bars, as standard errors of the mean and equivalent to ± 1 s (Fitzsimons *et al.*, 2000) are given for the C isotope ratio. Errors for the N are often smaller than the symbol (see Table 4 for compilation) and are not shown.

CATHODOLUMINESCENCE CHARACTERISTICS

TABLE 4. N abundance data on Bultfontein diamond J/1063.1 ('whopper')

CL zone	Analysis point*	N content (wt ppm)	1 s (\pm) (wt ppm)**	N content (atomic ppm)
Transect one (top left to bottom right, Fig. 3a)				
C2	34	654	20	561
B	33	7	0	6
B	32	3	0	3
A2	31	670	21	574
A2	30	941	29	807
A2	29	889	28	762
A1	28	978	31	839
A1	27	1056	34	905
A1	1	1080	65	926
A1	2	1143	68	980
A1	3	1235	73	1060
A1	4	997	57	855
A1	5	999	56	856
A2	6	715	40	613
B/C1	8	104	5	89
B/C1	7	60	3	52
C1	9	769	39	659
C2	10	635	31	544
C4	11	441	22	378
D1	12	354	16	303
D1	13	450	21	386
D2	14	586	28	503
D2	15	475	21	407
D2	16	530	24	454
D2	17	527	22	452
D2	22	629	23	540
D2	18	528	22	453
D2	21	1305	50	1119

repeated traverses were made with the specific objective of examining whether any variation in $\delta^{13}\text{C}$ could be found, which might correlate with the narrow octahedral subzones showing contrasting CL in this part of the specimen. A moderate number of the analysis points fall on subzone boundaries as well as within subzones in Fig. 4c, because the ion microprobe analyses are performed 'blind', in that the CL subzones cannot be seen during ion microprobe analysis.

The individual subzones, identified as a, b, c, d, e, f, g (Figs 4b,c), clearly show ranges of overlapping values. Focusing on subzone D2e, for which there is the largest number of measurements, there is a range of values of $\delta^{13}\text{C}$ from -7.3 to -2.8‰ (Table 5, Fig. 4b). This range is virtually identical to that of -7.5 to -2.3‰ for the whole of zone D (ignoring the two obviously outlying values which we treat as aberrant measurements). The range of 4.5‰ in

TABLE 4. (contd.)

CL zone	Analysis point*	N content (wt ppm)	1 s (\pm) (wt ppm)**	N content (atomic ppm)
D2	19	1368	55	1173
D2	20	467	19	401
Transect two (from bottom towards centre, Fig. 3a)				
C1	23	887	32	761
C1/B	24	419	20	359
B	25	6	0	5
A2/B	26	66	11	57
Transect three (from upper right towards centre, Fig. 3a)				
C2	38	567	17	487
C1	37	536	17	460
C1/B	36	490	16	420
B	35	4	0	4
A2	39	805	26	690
A2	40	810	25	694
A2	41	757	23	649

* Analysis points are numbered according to their order of collection for each transect; but they are listed in the order of their distribution along each transect as stated; points shown on Fig. 3a.

**Errors are standard errors of the mean for measurements (50 cycles) made on each point and taking into account variation in the standard value during a continuous analytical session; they do not include error in the absolute value of the standard as determined by combustion.

our measurements of zone D2e corresponds closely with a range of 4.2‰ , which is given by three times the average (Table 5) standard deviation ($3s = 3x \pm 0.7\text{‰}$), and we believe represents the overall precision for the ion microprobe analyses. It is important to note that although ± 0.7 is an average $\pm 1s$ value of precision (Table 5) for measurements made during a single period of analysis, it is the minimum to be expected in comparing measurements made in separate time periods of analysis, when electron multipliers and their settings were different and different standards were used (Fig. 1, this paper; Harte and Otter, 1992; Fitzsimons *et al.*, 2000). This interpretation of the range of values obtained for D2e is strongly supported statistically. A two sample *t* test comparing zone D2e with the combined data of all other D subzones, shows virtually identical distributions with $t = 0.02$ and $p = 0.98$. If there is

TABLE 5. C isotope data for Bultfontein diamond J/1063.1 ('whopper')

CL zone	Analysis Point*	$^{13}\text{C}/^{12}\text{C} \times 10^{-2}$		$\delta^{13}\text{C}$	
		value	1 s (\pm)**	‰PDB	1 s (\pm)***
Transect one (long transect, upper left to bottom right, Fig. 3a)					
C2	23	1.069	0.0007	-6.19	0.68
B	20	1.069	0.0006	-6.21	0.60
B	21	1.070	0.0008	-5.44	0.71
A2	24	1.069	0.0007	-6.72	0.64
A2	25	1.070	0.0007	-5.30	0.67
A2	26	1.069	0.0007	-6.53	0.62
A1	27	1.070	0.0007	-5.48	0.65
A1	28	1.069	0.0007	-6.88	0.63
A1	2	1.069	0.0006	-7.13	0.63
A1	1	1.072	0.0007	-3.88	0.66
A1	12	1.071	0.0007	-5.16	0.66
A1	11	1.070	0.0006	-5.54	0.61
A1	83	1.080	0.0006	-5.82	0.68
A1	3	1.069	0.0007	-6.48	0.68
A1	82	1.078	0.0007	-7.39	0.74
A1	81	1.080	0.0006	-5.89	0.67
A2	5	1.069	0.0007	-6.60	0.68
A2	4	1.071	0.0007	-5.25	0.66
A2	80	1.079	0.0006	-6.96	0.64
A2	8	1.071	0.0007	-5.14	0.66
B	7	1.071	0.0007	-5.04	0.69
B	15	1.071	0.0007	-5.29	0.68
B	18	1.070	0.0007	-5.50	0.63
B	77	1.081	0.0007	-4.67	0.67
B/C1	9	1.070	0.0008	-5.61	0.75
B/C1	14	1.071	0.0007	-5.08	0.67
C1	22	1.071	0.0006	-4.50	0.59
C1	79	1.081	0.0007	-4.69	0.70
C1	76	1.082	0.0007	-3.98	0.67
C1	78	1.083	0.0007	-3.41	0.70
C1	6	1.071	0.0007	-5.07	0.68
C2	75	1.080	0.0007	-5.78	0.66
C2/C4	74	1.081	0.0008	-5.23	0.74
D1	73	1.082	0.0006	-4.62	0.64
D1	72	1.083	0.0008	-3.40	0.76
D1	16	1.072	0.0007	-4.21	0.64
D2b/c	71	1.079	0.0008	-7.24	0.76
D2b/c	86	1.080	0.0007	-5.63	0.76
D2c/d	19	1.073	0.0007	-3.36	0.69
D2d	70	1.080	0.0007	-6.01	0.73
D2d/e	10	1.074	0.0007	-2.32	0.70
D2d/e	85	1.079	0.0007	-6.65	0.72
D2e	13	1.073	0.0006	-2.82	0.58
D2e	84	1.081	0.0007	-4.23	0.78
D2e	69	1.081	0.0007	-5.36	0.73
D2e	87	1.079	0.0007	-6.22	0.75
D2e	17	1.071	0.0007	-4.72	0.65
D2f	68	1.081	0.0007	-5.25	0.78

CATHODOLUMINESCENCE CHARACTERISTICS

TABLE 5. (contd.)

CL zone	Analysis Point*	$^{13}\text{C}/^{12}\text{C} \times 10^{-2}$		$\delta^{13}\text{C}$ ‰PDB	$\delta^{13}\text{C}$ ‰
		value	1s (\pm)**		
Transect two (short transect in bottom right, central linear transect of Fig. 4c)					
D2b	34	1.071	0.0006	-4.69	0.57
D2c	33	1.071	0.0007	-4.74	0.64
D2d/e	32	1.073	0.0006	-2.97	0.59
D2e	31	1.071	0.0007	-4.47	0.64
D2e	30	1.071	0.0007	-4.41	0.62
D2e/f	29	1.070	0.0007	-5.45	0.67
D2f/g	35	1.070	0.0006	-5.16	0.61
D2g	36	1.072	0.0007	-3.62	0.70
D2g	37	1.079	0.0007	2.59	0.64
Transect three (short transect in bottom right, extreme right side transect of Fig. 4c)					
D2c/d	42	1.070	0.0007	-5.17	0.67
D2e	41	1.071	0.0007	-4.54	0.64
D2e	40	1.069	0.0006	-6.28	0.62
D2e	39	1.071	0.0007	-4.90	0.71
D2e/f	38	1.070	0.0007	-5.61	0.63
Transect four (short transect in bottom right, next to right hand transect of Fig. 4c)					
D1	43	1.071	0.0007	-4.69	0.71
D2a	44	1.070	0.0007	-5.79	0.64
D2a	45	1.068	0.0007	-7.11	0.70
D2a	45R	1.068	0.0007	-7.53	0.67
D2b	46	1.071	0.0006	-4.82	0.56
D2c/d	47	1.070	0.0006	-4.95	0.63
D2e	48	1.068	0.0007	-7.35	0.68
D2e	49	1.070	0.0007	-5.77	0.70
D2e	50	1.070	0.0006	-5.61	0.63
D2e	51	1.072	0.0007	-3.91	0.65
D2f	52	1.070	0.0006	-5.32	0.64
D2g	53	1.069	0.0007	-6.14	0.67
D2g	54	1.070	0.0007	-5.03	0.66
Transect five (short transect in bottom right, central 7-point transect of Fig. 4c)					
D2a	61	1.008	0.0006	-6.40	0.76
D2b	60	1.011	0.0007	-4.58	0.82
D2c	59	1.012	0.0007	-4.72	0.82
D2e	58	1.011	0.0006	-6.49	0.76
D2e	57	1.014	0.0006	-4.72	0.76
D2f	56	1.013	0.0007	-6.10	0.77
D2g	55	1.016	0.0007	-4.62	0.78
Transect six (short transect in bottom right, extreme left side of transect of Fig. 2c)					
D2b	62	1.006	0.0007	-4.51	0.95
D2d	63	1.005	0.0005	-4.15	0.84
D2e	64	1.005	0.0007	-3.29	0.95
D2e	65	1.003	0.0006	-4.12	0.93
D2e	66	1.003	0.0007	-2.90	1.04
D2f/g	67	1.004	0.0008	-1.12	1.11

* as for Table 4; points shown on Figs 3a and 4c.

** and *** as for Table 3.

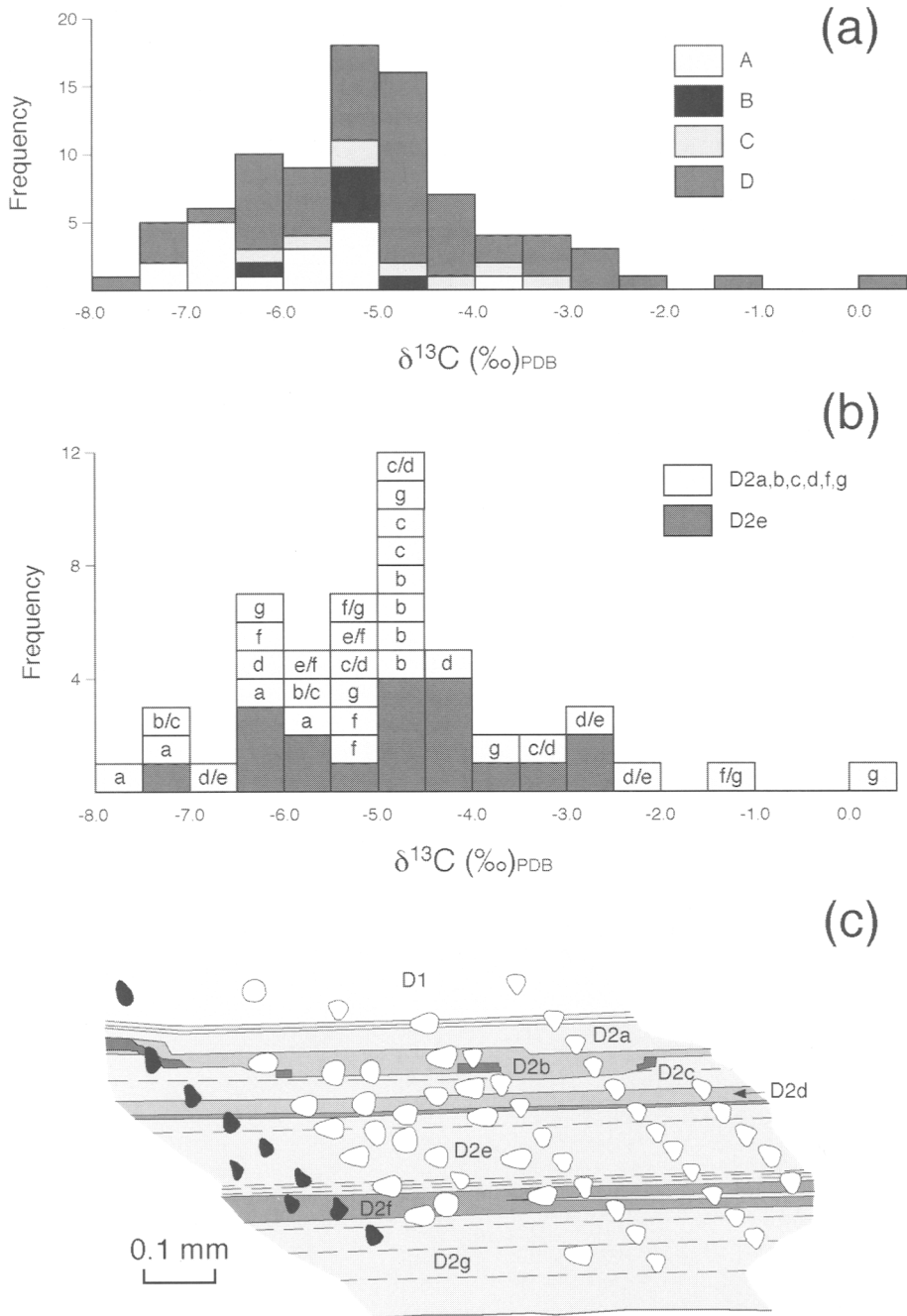


FIG. 4. Plots of $\delta^{13}\text{C}$ ‰ data for the 'whopper' diamond. (a) Histogram of all data for the diamond with analytical points for major zones A, B, C, D of Fig. 3a distinguished. (b) Histogram of analytical points in the bottom right area of the diamond as seen in Plate 2a and Fig. 3a and further detailed in Fig. 4c. (c) Positions of ion microprobe pits for measurements made in repeated transects across bottom right of diamond (Plate 2a and Fig. 3a, and as tabulated in Tables 5 and 6). Pits in white were made for $\delta^{13}\text{C}$, pits in black were for N.

any real variation in $\delta^{13}\text{C}$, the data suggest it is as great within the subzones as between them.

In summary, the results for the 'whopper' show that there is probably a small but distinct difference in C isotope composition between zone A and zones C+D, with zone B having intermediate values. Compositions are closely similar between major zones and subzones in C+D, including the narrow octahedral subzones of contrasting CL.

Koffiefontein specimen K3
CL characteristics

Plate 2b and Fig 5a show that this diamond is strongly dominated by octahedral growth. It appears to have two 'seed' crystals, referred to

as A and B in Fig. 5, though it is possible that they become joined as a single seed out of the plane of section. Surrounding the seeds is a broad zone of fairly homogenous CL (zone C), which gives way in the outer part of the crystal to a complex zone (D) where there are alternating bright and dark blue CL zones of dominantly octahedral character (Plate 2b).

N and $\delta^{13}\text{C}$ data

The measurements, arranged in two transects across the crystal at right angles, are presented in Tables 6 and 7 and Fig. 5. Nitrogen (Table 6) varies from 3 to 347 ppm (by weight), with abundance correlating closely with the CL zones (cf. Plate 2b and Fig. 5). Marked variations in measured N_{ppm} may be seen in zones A, B and D,

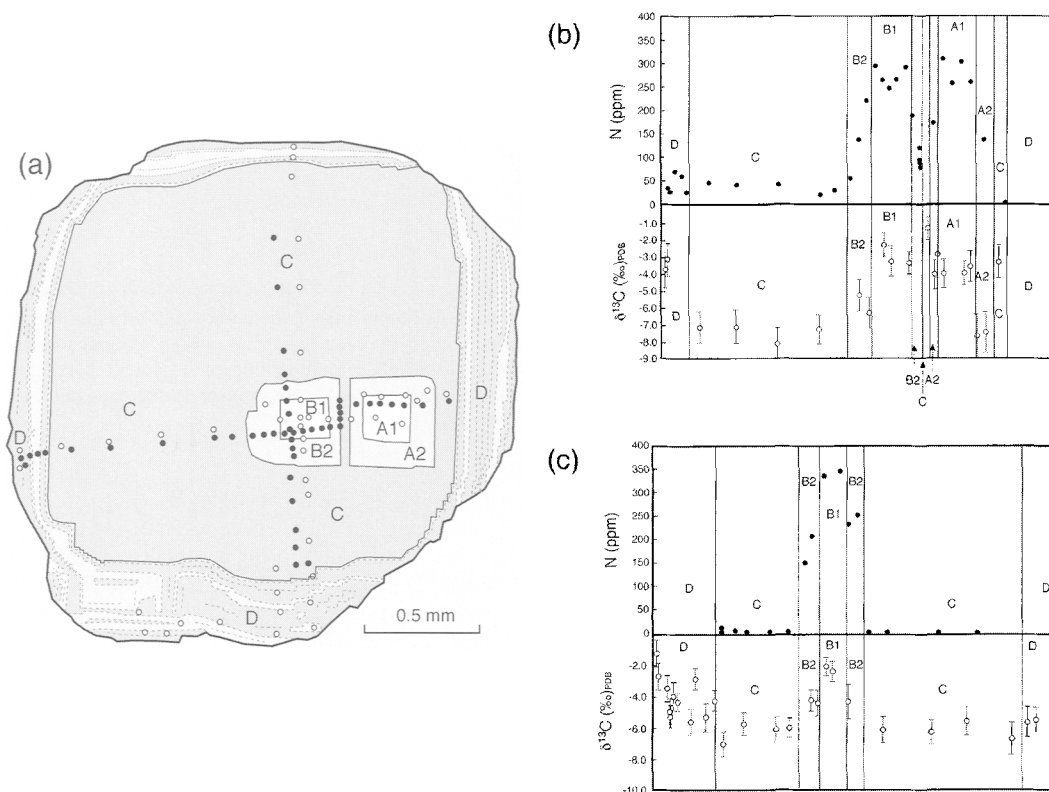


FIG. 5. CL zones with N and $\delta^{13}\text{C}$ ‰ for the Koffiefontein K3 diamond (see also Plate 2b). (a) Summary of the major sets of CL zones (A, B, etc) and subzones (B1, B2, etc) as seen in CL, together with the positions of ion microprobe analysis points (solid dots being for N abundance and open circles for C isotope ratio) corresponding with data given in Figs 5b and 5c (below) and Tables 6 and 7. (b) and (c) show N_{ppm} (by weight) and $\delta^{13}\text{C}$ ‰ respectively, for the analysis points of the left-right and bottom-top transects of Fig. 5a. Error bars, as standard errors of the mean and equivalent to ± 1 s (Fitzsimons *et al.*, 2000) are given for the C isotope ratio. Errors for the N are often smaller than the symbol (see Table 6 for compilation) and are not shown.

TABLE 6. N abundance data for Koffiefontein K3 diamond

CL zone	Analysis point*	N content (wt ppm)	1 s (\pm) (wt ppm)**	N content (atomic ppm)
Transect one (from right to left across diamond as seen in Fig. 5)				
C	1	4	0	3
A2	2	138	8	118
A1	3	260	15	223
A1	4	303	19	260
A1	5	257	14	220
A1	6	310	17	266
A2	7	173	9	149
B2	8	78	4	67
B2	9	119	6	102
B2	10	95	5	82
B2	11	88	5	75
B2	12	79	4	68
B2	13	189	10	162
B1	14	291	15	250
B1	15	264	13	227
B1	16	247	13	212
B1	17	263	13	226
B1	18	293	15	251
B2	19	220	11	188
B2	20	138	7	118
B2	21	56	3	48
C	22	31	2	27
C	23	22	1	19
C	24	42	2	36
C	25	42	2	36
C	26	46	2	39
D	27	26	1	22

TABLE 6 (contd.)

CL zone	Analysis point*	N content (wt ppm)	1 s (\pm) (wt ppm)**	N content (atomic ppm)
D	28	60	3	52
D	29	69	4	60
D	31	27	2	23
D	30	35	2	30
Transect Two (from bottom to top across diamond as seen in Fig. 5)				
C	32	12	1	10
C	33	3	0	3
C	34	5	0	5
C	35	3	0	3
C	36	4	0	3
C	37	5	0	4
B2	38	151	10	130
B2	39	208	14	178
B2	40	244	17	209
B1	41	336	24	288
B1	42	347	27	297
B2	43	234	18	200
B2	44	253	20	217
C	45	3	0	2
C	46	4	0	4
C	47	4	0	4
C	48	4	0	4

* Analysis points are numbered according to their order of collection for each transect, but they are listed in the order of their distribution along each transect starting at the right or bottom of each transect as seen in Fig. 5a.
** as for Table 4.

which have multiple CL subzones of varying brightness, whilst zone C of uniform relatively low CL intensity consistently shows <50 ppm N.

The $\delta^{13}\text{C}$ data for this crystal have been reported previously (Harte and Otter, 1992) and are reproduced here as Table 7 (all values have a small displacement with respect to the Harte and Otter numbers, due to re-computation following redetermination of the standard composition – see methods section). As noted by Harte and Otter (1992), K3 does show some correlation of $\delta^{13}\text{C}\text{‰}$ with CL and therefore with growth zones. The relatively broad zone C, with a mean of -6.4‰ $\delta^{13}\text{C}\text{‰}$ and most data clustered between -5.6 and -7.2‰ , appears reasonably distinct from the ‘seed’ crystals. The ‘seeds’ show a fairly wide spread of values, but have generally heavy cores (A1 with a mean of -3.7 and B1 with a mean of -2.8‰). Despite its multiple growth layers, zone

D shows a reasonably tight grouping of $\delta^{13}\text{C}$ values with an intermediate mean of -4.13‰ .

A two sample t test (95% confidence limits) of C and D gives $t = -4.7$, $p = 0.0001$ and strongly substantiates the two zones being non-equivalent in $\delta^{13}\text{C}$. A similar result ($t = 4.7$, $p = 0.0002$) is obtained if ‘seed’ B, for which there is most data, is compared with zone C. Interestingly, although the numbers of analyses must be noted as small for seed A, a t test suggests there is no distinction between the means of all analyses for the two ‘seeds’, A and B, and this might support their junction out of the plane of the section.

Thus the Koffiefontein K3 diamond shows much more evidence of differences in $\delta^{13}\text{C}$ than the Bultfontein diamonds described above. It is also notable that zone C, which seems to be essentially one growth zone with almost constant CL, shows the tightest grouping of $\delta^{13}\text{C}\text{‰}$.

CATHODOLUMINESCENCE CHARACTERISTICS

TABLE 7. C isotope data for Koffiefontein K3 diamond

CL zone	Analysis point*	$^{13}\text{C}/^{12}\text{C} \times 10^{-2}$		% ‰_{PDB}	$\delta^{13}\text{C}$ 1 s (\pm)***
		value	1 s (\pm)**		
Transect one (from right to left across diamond as seen in Fig. 5)					
C	1	1.073	0.0010	-3.45	0.98
A2	2	1.068	0.0012	-7.54	1.18
A2	4	1.068	0.0013	-7.76	1.26
A1	3	1.072	0.0009	-3.73	0.88
A1	44	1.074	0.0007	-4.12	0.69
A1	43	1.074	0.0009	-4.14	0.84
A1	5	1.073	0.0015	-3.01	1.41
A2/A1	6	1.071	0.0009	-4.18	0.88
A2/C	45	1.077	0.0007	-1.47	0.71
B1	46	1.075	0.0007	-3.49	0.67
B1	42	1.075	0.0009	-3.39	0.87
B1	41	1.076	0.0007	-2.43	0.70
B2	9	1.073	0.0009	-6.39	0.90
B2	7	1.070	0.0010	-5.36	0.96
C	10	1.072	0.0009	-7.33	0.86
C	11	1.071	0.0009	-8.13	0.88
C	12	1.073	0.0010	-7.16	0.97
C	13	1.073	0.0009	-7.16	0.90
D	15	1.077	0.0010	-3.16	0.97
D	14	1.076	0.0011	-3.75	1.05
Transect two (from bottom to top across diamond as seen in Fig. 5)					
D	16	1.079	0.0009	-1.19	0.89
D	18	1.078	0.0009	-2.68	0.90
D	19	1.077	0.0009	-3.45	0.87
D	20	1.075	0.0009	-4.94	0.84
D	17	1.075	0.0008	-5.26	0.74
D	21	1.076	0.0010	-3.96	0.96
D	25	1.070	0.0006	-4.32	0.70
D	22	1.075	0.0009	-5.64	0.88
D	26	1.072	0.0007	-2.88	0.74
D	23	1.075	0.0010	-5.31	0.97
C/D	27	1.070	0.0007	-4.27	0.69
C	24	1.073	0.0009	-7.03	0.86
C	28	1.069	0.0008	-5.78	0.78
C	29	1.069	0.0009	-6.11	0.84
C	49	1.072	0.0007	-6.01	0.70
B2	48	1.074	0.0007	-4.25	0.74
B2	30	1.070	0.0009	-4.45	0.89
B1	47	1.076	0.0006	-2.08	0.65
B1	41	1.076	0.0007	-2.43	0.70
B2	8	1.071	0.0012	-4.36	1.22
C	31	1.069	0.0009	-6.15	0.90
C	32	1.069	0.0008	-6.36	0.83
C	33	1.069	0.0010	-5.64	0.99
C	34	1.068	0.0011	-6.70	1.13
D	35	1.070	0.0010	-5.67	1.05
D	36	1.070	0.0009	-5.54	0.92

* as for Table 6; ** and *** as for Table 3.

Discussion

Nitrogen abundances and CL characteristics

Previous luminescence and spectroscopy studies on diamonds have shown the dependence of CL characteristics on defects and, in particular, N impurities and their aggregation state (Davies, 1974; Marfunin, 1979; Burns *et al.*, 1990). The present data for natural diamonds confirm in detail that the variations in CL, which make the growth zones apparent, are closely associated with variations in the abundance of N. Measurements on growth zones in all three diamonds show that each zone has particular N abundance characteristics. In general, the brightness of blue CL increases with increasing N content. In the case of the 'wild-one' the available FTIR data indicate that this correlation applies with constant N aggregation state. Shades of yellow or green in the 'wild-one', often occur with very low N abundances; these colours are usually associated with deformation effects, and perhaps become manifest in the low N zones because they are not dominated by the blue luminescence. Clearly, there is a basis for correlating particular CL characteristics with N abundance and aggregation state, but establishing a quantitative calibration of these parameters requires specification of the CL response in terms of light wavelength and intensity for specific operating conditions (Davies, 1974; Marshall, 1988; Burns *et al.*, 1990; Clarke *et al.*, 1992).

Nitrogen abundances and growth orientation

Although N abundances obviously vary dramatically between growth layers, they show no overall correlation in the present cases with the shape and orientation of growth zones. Cuboid and octahedral growth zones may both have high and low N contents, and sharp fluctuations of N abundance occur across narrow zones in all the diamonds irrespective of growth orientation. Occasionally a local pattern is seen, as in zones C and D of the 'wild-one' where a progressive drop in N abundance has occurred during growth on curved cuboid 'faces'. In the present diamonds, it also seems to be the case that sharp fluctuations in both CL and N occur more commonly in octahedral than cuboid growth zones. This is seen in a comparison of cuboid zones such as B, C and D of the 'wild-one' and A, B and C of the 'whopper', with the outer octahedral growth zones of the 'whopper' and K3. This may be

partly a reflection of the differences in rates of growth and N uptake of cuboid and octahedral faces/surfaces (Sunagawa, 1984; Burns *et al.*, 1992). A change in N availability and uptake during growth may tend to have a more marked effect on octahedral than cuboid growth zones, because of greater uptake of N by octahedral faces and their slower rate of growth compared with cuboid faces (Lang, 1974a; Sunagawa, 1984).

For the specific case of comparing simultaneous growth of both octahedral and cuboid layers, the present diamonds can provide little evidence, because they do not show a clear situation like that of the 535A diamond described by Lang (1974a), where sharp changes in CL and presumably N_{ppm} occur in apparently continuous growth layers passing from octahedral to cuboid sectors. However, it is possible that the sharp octahedral re-entrant faces, seen on the inside of zones D and E of the 'wild-one' (Plate 1 and Fig. 2a, right side), were forming extremely slowly at the same time as the cuboid growth subzones beside them were developing outwards. In this case there is a very marked contrast between the strong luminescence of the octahedral zone and the variable and weak luminescence of the adjacent cuboid zones (C2, C3, D2, D3), which would correspond with the higher N contents of octahedral compared with cuboid growth sectors observed by Lang (1974a) and Burns *et al.* (1990).

Variation of $\delta^{13}C$ with CL and N

Patterns of variation in $\delta^{13}C$ are hard to discern in the 'wild-one' and the 'whopper' diamonds. This is largely because the range of variation is often close to detection limits and statistical distinctions in $\delta^{13}C$ between CL zones and subzones are difficult to establish. In K3, where distinct differences in $\delta^{13}C$ are seen, the zones (A, B, C, Fig. 5) show a broad correlation of decreasing CL and N with decreasing $\delta^{13}C$, but there are evident exceptions (e.g. subzone A2). In the 'whopper' the consistently highly luminescent inner zone has slightly lower $\delta^{13}C$ than other zones, which is the opposite of the rough trend seen in K3.

Most spectacularly, the 'wild-one' shows wide variations in N abundance between CL subzones, but no concomitant variations in $\delta^{13}C$. Similarly, the outer parts of the 'whopper' and K3 show narrow octahedral zones with little or no variation in $\delta^{13}C$, but marked changes in CL and variations in N_{ppm} of c. 50–300 (Tables 2, 4, 6, and Figs 2,

4, 5). This marked lack of evidence of any correlation between $\delta^{13}\text{C}$ and N abundance is further discussed in the following sections.

N and $\delta^{13}\text{C}$ in relation to growth history

All three diamonds show features suggestive of changing conditions of growth, as shown particularly by the marked boundaries dividing major growth zones in all three diamonds. Within the delineated major growth zones there may be evidence of fairly constant, gradually changing, or abruptly changing conditions. Relative constancy of CL luminescence, N and $\delta^{13}\text{C}$ is seen in zones A of the 'whopper' and C of K3. Thus the fluid reservoir from which the diamonds were growing appears to have remained unaffected by fractionation or depletion during these periods of relatively extensive growth. Therefore, the fluid reservoir was sufficiently large to be unaffected by diamond crystallization, and the diamonds grew in an open system. In the 'wild-one' gradual changes within each of zones B, C and D, marked by decreasing luminescence and falling N_{ppm} , might suggest a gradual depletion of the fluid source reservoir in N. We see no patterns in the ion microprobe $\delta^{13}\text{C}$ data variation which might be linked to fractionation effects or progressive changes in oxygen fugacity during growth of the type modelled by Deines (1980).

Where changes in CL and N_{ppm} accompany change in growth orientation, care in interpretation is clearly necessary. Thus the gradual changes within zones B, C and D of the 'wild-one' noted above are terminated by sharp changes in CL luminescence, N_{ppm} and the change of growth zone orientation from cuboid to octahedral. It is difficult to say whether these abrupt changes reflect straightforward changes in the fluid reservoir from which the diamonds grew, or whether they also reflect changes in growth rate and uptake of N in the cuboid to octahedral transition (Lang, 1974a; Sunagawa, 1984; Burns *et al.*, 1990; Satoh *et al.*, 1990; Taylor *et al.*, 1996).

However, all three diamonds also show conspicuous examples of changes in CL and N across major and minor zone boundaries, which are not simultaneously marked by a change in growth zone orientation (either cuboid or octahedral, but most often the latter). Such abrupt variations in N uptake during growth in a constant orientation suggest fluctuations in the fluid reservoir during growth.

The lack of change in $\delta^{13}\text{C}$ between many growth zones where abrupt changes occur in CL and N_{ppm} suggests that the controls for N_{ppm} and $\delta^{13}\text{C}\text{‰}$ during diamond growth from the fluid/melt reservoir are often independent. This conclusion appears to be widely applicable. Lack of correlation between $\delta^{13}\text{C}$ and N abundance is also seen on the small scale in the ion microprobe study of George Creek stones (Fitzsimons *et al.*, 1999), and is a general conclusion of large scale geochemical analysis of whole natural diamonds (Deines *et al.*, 1991, 1993). From the studies of Burns *et al.* (1990), and our measurements on synthetic diamond standards (see Methods section), it appears that constancy of $\delta^{13}\text{C}\text{‰}$ and variability in N_{ppm} in individual diamonds is also true for synthetic diamonds.

However, although constancy of $\delta^{13}\text{C}$ during growth of diamond crystals is clearly common, it is evident from K3 and the George Creek diamonds (Fitzsimons *et al.*, 1999) that changes in $\delta^{13}\text{C}$ during diamond growth can occur. This raises another question – are there circumstances where the mobility of C atoms within the diamond lattice could remove differences in C isotope distribution by 'random-walk' diffusion? In other words, rather than attributing all cases of constant $\delta^{13}\text{C}$ across distinct CL growth zones to constancy during crystal growth, are there possibly cases where $\delta^{13}\text{C}$ has been homogenized after growth?

Atomic mobility and N aggregation

Expressed in terms common in the Earth Science literature, the suggestion that diffusion causes homogenization of isotope compositions, is equivalent to saying that the diamonds experienced temperature-time conditions above the 'closure temperature' (Dodson, 1986) for C element/isotope mobility. Clearly this possibility merits consideration, given that most evidence suggests formation of diamonds in the deep lithosphere or asthenosphere at temperatures of 950°C or more, and that the diamonds may well have remained at such temperatures for many millions of years (Meyer, 1987; Harris, 1987, 1992; Gurney, 1989). Consideration of C mobility inevitably involves consideration of N mobility, and it is clear from our data that any mechanism for homogenizing C distribution must be accompanied by a mechanism preventing wide-scale redistribution of N, whose variable abundance appears to reflect original growth patterns.

This contrast in behaviour of C and N atoms may be related to the fact that N in natural diamonds is typically found in aggregates of atoms, even though there is considerable evidence to suggest that N initially becomes incorporated in the diamond lattice as single atoms substituting for C (e.g. Evans, 1992; Mainwood, 1994; Taylor *et al.*, 1996). Available evidence suggests that the mobility of such single impurity atoms will be similar to that of single C atoms in the diamond lattice (e.g. Stoneham, 1992; Mainwood, 1994). Thus, at the time of diamond growth, the mobility of C and N atoms in N-bearing (Type I) diamonds will be closely similar, but subsequent differences arise because the mobility of the N leads to N atoms meeting and forming: (1) pairs (the IaA aggregation state); (2) aggregates of four atoms plus a vacancy (the IaB aggregation state); or (3) combinations of three atoms or platelets. Experimental work suggests that the movement of single N atoms at first leads dominantly to the A aggregation state and then to the higher aggregation states (Evans, 1992; Taylor *et al.*, 1996).

The fact that N commonly changes from single atom to the IaA and higher aggregation states in natural diamonds, clearly means that conditions of residence after growth in the Earth's mantle favour N atomic mobility. With similarity between single C and N atoms, the conditions of residence must also favour C atomic mobility, which would lead towards homogenization of C isotope compositions. The big difference between N and C is that the aggregation of N leads to its relative stabilization, because the mobility of aggregated N has a higher activation energy than that of single N atoms. Furthermore, even at low N concentrations the distances of atomic movement necessary to achieve pairing of N atoms are very small (Taylor *et al.*, 1996). With only 50_{ppm} N, and eight atoms per diamond unit cell of cell edge 3.57 Å, a single N atom has only to move on average 2500 unit cells, or <1 μm, in order to encounter another N atom. Thus the original variations in N distribution associated with growth zones will become stabilized on a scale smaller than the growth zones by aggregation processes. In effect the initial similarity in C and N diffusion rates, is removed by only a very small distance of N mobility. The question now arises of whether the magnitudes of the diffusion parameters are sufficient to remove heterogeneities in C isotope composition on the scale of the growth zones in natural crystals.

Diffusion data on diamonds

The diffusion mechanisms and diffusion rates in diamond have been addressed by a number of researchers in the physical sciences because the distribution and mobility of impurity atoms (particularly B and N) in the diamond atomic structure affects the optical, electrical and electron paramagnetic resonance (EPR) properties of diamonds (e.g. Swalin, 1961; Chrenko *et al.*, 1977; Stoneham, 1992; Mainwood, 1994). From the geological-mineralogical viewpoint, the study of N mobility and its effect on the state of aggregation of N atoms in natural diamonds has provided potential evidence on the time-temperature history of diamonds (e.g. Chrenko *et al.*, 1977; Evans and Harris, 1989; Taylor *et al.*, 1990, 1996; Richardson and Harris, 1997).

The governing energies for diffusion of single atoms of impurities like B and N are expected to be similar to those for self diffusion of C atoms, and the diffusion in all cases involves the motion of substitutional atoms on lattice sites (e.g. Evans, 1992; Stoneham, 1992; Mainwood, 1994). Thus studies of the rates of N aggregation from single substitutional atoms, or of B diffusion, simultaneously provide evidence on rates of diffusion of atomic C in the diamond lattice. Stoneham (p. 21, 1992) notes that all experimentally-determined substitutional impurity diffusion rates are broadly similar and quotes a general value of $D = 3 \text{ cm s}^{-1} \exp(-2.47 \text{ eV}/kT)$ where: D is diffusion rate, and k is Boltzmann's constant, with T in Kelvin. Compared to individual estimates, this generalized rate seems to be rather high (Fig. 6).

In comparing sets of experimental data it is important to note that experiments involving N diffusion have not been so much directed at measuring diffusion rate in relation to distance, but the rate of aggregation of N atoms in Type Ib diamonds (with single N atoms substituting for C) to form Type IaA diamonds (with N in pairs of neighbouring substitutional atoms). Clearly these data provide important evidence on the mobility of single atoms of appropriate atomic radius. However, the experiments have usually been conducted on synthetic and natural diamonds, which as we have seen characteristically show variable N concentration in different growth zones, and have probably measured average rates of aggregation across a number of growth zones using IR spectroscopic techniques (Chrenko *et al.*, 1977; Evans, 1992; Taylor *et al.*, 1996). Thus, although these data provide evidence on the

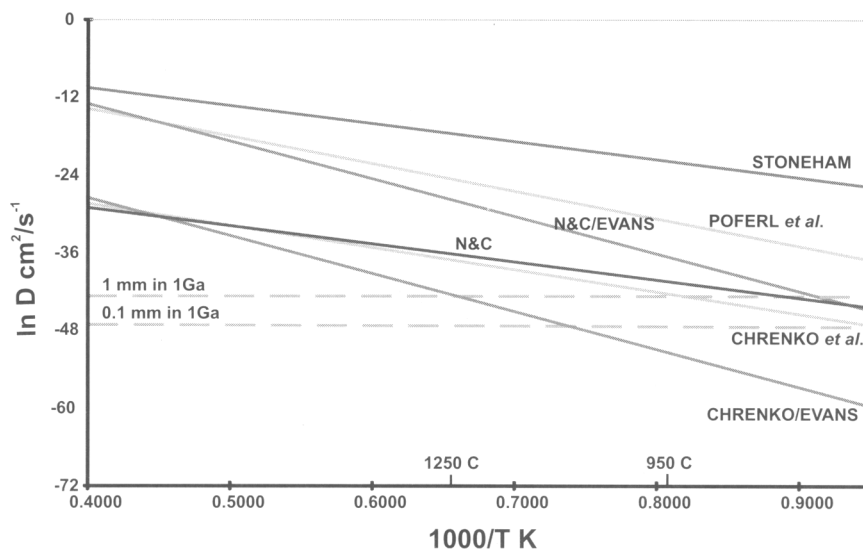


FIG. 6. Arrhenius plot of diffusion data for diamonds. The data in solid lines are taken from: Chrenko *et al.*, 1977; Narducci and Cuomo, 1990; Poferyl *et al.*, 1973; Stoneham, 1992. The data lines labelled with multiple authors (Chrenko/Evans, and N&C/Evans) use estimates of the diffusion coefficient at high temperature (from Chrenko *et al.*, 1977) and at low temperature (from Narducci and Cuomo, 1990) respectively, combined with the estimate of activation energy given by Evans (1992). Horizontal dashed lines are estimates of natural log values of the minimum diffusion coefficients necessary to achieve virtually complete homogenization of C isotopes by diffusion on the scale of 1.0 mm and 0.1 mm. See text for further details.

activation energies of diffusion, they only provide indirect evidence on the length scales of diffusion and the value of the pre-exponential constant in the diffusion rate equation for motion of single atoms. The data for B diffusion in diamond do not appear to be complicated by aggregation, though here again studies emphasize measurement of activation energy (Wentorf and Bovenkerk, 1962) rather than diffusion rate. Narducci and Cuomo (1990), however, provide data on B diffusivity at the remarkably low temperature of 800°C using a method of impedance spectroscopy.

Experimental estimates of single atom N and B diffusion, and therefore C diffusion, are given in Fig. 6, together with the generalized value of Stoneham (1992) referred to above. All the data are essentially 'order-of-magnitude' determinations. The Poferyl *et al.* (1973) data use the Wentorf and Bovenkerk (1962) value of activation energy over 1500–2000°C and estimate diffusion distance at 2000°C to give: $D = 22 \text{ cm}^2 \text{ s}^{-1} \exp(-80000 \text{ cal}/RT)$ or $D = 22 \text{ cm}^2 \text{ s}^{-1} \exp(-3.7 \text{ eV}/kT)$. Narducci and Cuomo (1990) determine D at 800°C and coupled with an estimate from Vasilov (1978) at 1200°C

effectively give $D = 3.02 \times 10^{-8} \text{ cm}^2 \text{ s}^{-1} \exp(-2.5 \text{ eV}/kT)$. The Chrenko *et al.* (1977) data use N aggregation rate together with computations of N distribution to yield $D = 7.07 \times 10^{-8} \text{ cm}^2 \text{ s}^{-1} \exp(-2.7 \text{ eV}/kT)$. The similarity of the Chrenko *et al.* (1977) and Narducci and Cuomo (1990) determinations is notable, and is particularly striking given that the determinations of the pre-exponential constants are respectively dependent on high and low temperature experimental data.

All the above data giving both pre-exponential constant and activation energy, have fairly similar negative activation energies in the range 2.5–3.7 eV. In comparison to the above, Evans (1992) argues strongly in favour of negative activation energies of ~5 eV on the basis of N aggregation experiments, and this somewhat higher value is supported by theoretical calculations of 4.5 eV for vacancy assisted N migration and 6.3 eV for direct atomic interchange (Mainwood, 1994). Most recently Taylor *et al.* (1996) have determined activation energies for N aggregation from Type Ib to Type IaA of 4.4 eV and 6.0 eV. These estimates are for octahedral

growth sectors and cube sectors respectively, which are thought to have different concentrations of vacancies and other defects. Considering that the experimental data involve average measurements of changing N aggregation in materials that would initially have had differing N concentrations in different growth zones (Chrenko *et al.*, 1977; Evans, 1992), their general consistency with one another and the calculated relationships (Mainwood, 1994) is remarkable. The only strongly dissenting note is given by the experimental results of Kanda *et al.* (1990), who determined an activation energy of 21 eV, but their results have been questioned by Taylor *et al.* (1996).

The effect of applying a higher negative activation energy, to some of the previously quoted estimates of diffusion rates, is shown in Fig. 6, using the Evans value of 5 eV, which is close to the average of these higher values. The Chrenko/Evans line, shown in Fig. 6, takes the high temperature estimate of D at 1900°C of Chrenko *et al.* (1977) and extrapolates it down temperature using the 5 eV value for activation energy, rather than the estimate of 2.7 eV (Chrenko *et al.*, 1977). Similarly the N&D/Evans line in Fig. 6, takes Narducci and Cuomo's (1990) estimate of D at 800°C and extrapolates up temperature with the Evans activation energy of 5 eV.

We can use the data from Fig. 6 to obtain order of magnitude estimates of the times for C diffusion and homogenization using the basic relationship $x^2=Dt$ where x is distance (characteristic length scale of diffusion), D is diffusion rate and t is time. From the viewpoint of distance we may note that narrow alternating bright-dark CL growth zones (e.g. outer parts of 'whopper' and K3) are commonly on a scale of <0.1 mm (Figs 3–5). Broader major growth zones may be ~1.0 mm across. In terms of residence times for the diamonds, then the ages of most Kaapvaal diamonds, other than cubic coated stones, have been determined as being in excess of 1.0 Ga (Richardson *et al.*, 1984, 1993; Burgess *et al.*, 1989; Smith *et al.*, 1991). Using $x^2=Dt$ we have calculated the values of D necessary to give diffusion on a scale of 0.1 and 1.0 mm with $t = 1.0$ Ga and plotted these values on Fig. 6 for comparison with the experimental and computed data for $\ln D$. In making this comparison we also have to consider likely temperatures of storage of diamonds in the mantle. Considering estimated geotherms and

xenolith geotherms, coupled with estimates from inclusions in diamonds, the most likely temperatures for diamondiferous deep lithospheric mantle beneath cratons are between 950 and 1250°C. (e.g. Boyd and Gurney, 1986; Meyer, 1987; Gurney, 1989; Rickard *et al.*, 1989).

Figure 6 shows that for a diffusion length of 0.1 mm (100 μm) in 1.0 Ga, temperatures of 950°C are more than adequate with all D estimates other than the Chrenko/Evans combination, which would require temperatures of ~1100°C. According to the Chrenko/Evans diffusion coefficients, diamonds would have to experience temperatures of ~1250°C for diffusion over a 1.0 mm distance, but the other data sets suggest a close approach to homogenization across 1.0 mm at 950°C or less. Clearly the range in determined D values leaves much room for error, which may be exacerbated by any variation in D due to lattice defects (Taylor *et al.*, 1996). Being conservative, one may say the diffusion data (Fig. 6) clearly point to the possibility that some Kaapvaal diamonds will have undergone homogenization of their C isotope composition on the 0.1 mm scale.

Conclusions

Multiple analyses on polished surfaces of transparent-blue diamonds with external octahedral growth forms, have revealed a pattern of wide variation in N_{ppm} , but only restricted variation in $\delta^{13}\text{C}$. Nitrogen frequently varies by >100 ppm on a scale of <100 μm , and differences of >500 ppm may occur on this scale. Variations in N abundance correlate with blue CL characteristics and the growth zones seen in CL. In purely relative terms, the brighter the blue CL luminescence, the higher the N content has usually been found to be.

Wide variations in N_{ppm} are seen in both cuboid and octahedral growth zones within the diamonds. Thus in one diamond, variations of N_{ppm} from 0 to 1000 are seen in cuboid growth zones, and 60 to 800 in octahedral growth zones. On the basis of their correlation with the CL growth zones, changes in N abundances are sharp on the micron scale, and increase and decrease repetitively during the growth history of the diamonds. They suggest the possibility of marked fluctuations in the availability of N from the fluid reservoir in which the diamonds are believed to have grown. In FTIR (Fourier transform infrared spectroscopy) studies, the determined N abun-

dances probably represent the average of several growth zones which may have widely different N_{ppm} . This may affect the calculation of aggregation rates and mantle residence times from knowledge of aggregation states.

In contrast to their N characteristics, all the diamonds show restricted variations in $\delta^{13}\text{C}$, which make it difficult to establish distinctions between growth zones by ion microprobe without multiple analyses or extremely long counting times. One diamond (K3) shows statistically significant differences of 2.3 to 3.6 $\delta^{13}\text{C}\%$ in the mean values of several major groups of growth zones. These differences are small compared with those seen in the exceptional George Creek diamonds (Fitzsimons *et al.*, 1999). In the Bultfontein diamonds examined, there are no sharp changes in $\delta^{13}\text{C}\%$ at major zone boundaries, and in all diamonds thin growth zones on the scale of 0.1 mm show little evidence of changes in $\delta^{13}\text{C}\%$ to accompany variations in N. This lack of correlation between N_{ppm} and $\delta^{13}\text{C}\%$ on the microscopic scale corresponds with the lack of correlation in these parameters at the macroscopic scale (Deines *et al.*, 1991, 1993), and shows a lack of correlation in the growth controls of N_{ppm} and $\delta^{13}\text{C}$.

Overall there are few patterns in either N_{ppm} or $\delta^{13}\text{C}\%$ which may be readily referred to aspects of crystal-fluid interaction during the diamond growth. A tendency for gradual depletion in N abundances for extensive zones of cuboid growth is seen in two diamonds; whilst sharp fluctuations in N content in narrow growth zones appear to be more common during octahedral growth. No zone or phase of growth preserves evidence of gradual continuous variations in $\delta^{13}\text{C}\%$ that might correspond to progressive variations in isotope composition as a result of fractionation and/or oxygen fugacity variation during diamond crystallization from a CH_4 or CO_2 reservoir, as modelled in the classic paper of Deines (1980).

In some cases it is possible that initial differences in $\delta^{13}\text{C}$ have been erased by diffusion. A mechanism for preserving composition differences in N, whilst not preserving them in C is well provided by the established tendency of single N atoms to aggregate, and once aggregated to become relatively immobile. Evidence of the longevity of diamonds over more than a thousand million years at high temperatures (~950–1250°C) within the Earth's mantle is well documented and under these conditions most experimentally determined diffusion coeffi-

cients predict homogenization of $\delta^{13}\text{C}$ on scales of at least 0.1 mm. Therefore, the diffusion rates appear to be such, that the scale of preservation or loss of C isotope composition heterogeneity in natural diamonds may provide evidence of the ages and temperatures of residence of diamonds within the mantle. Clearly such data might potentially be combined with that from investigation of N aggregation states by IR spectroscopy. However, these methods need more detailed controls, including: improvements in ion microprobe precision for C isotope analysis; close correlation of N abundance with aggregation state in commonly heterogeneous samples; and better knowledge of diffusion parameters.

Acknowledgements

A major contribution to this work was made by John Craven by his expert maintenance of the Edinburgh/NERC SIMS instrument and his help in the taking of the measurements and processing of the data. Apart from putting pen to paper, his effort means that he should really be the first author on this paper, but he has decided in principle that his role is to facilitate rather than report the use and development of SIMS techniques. Thanks are also due to De Beers Consolidated Mines, and John J. Gurney, for the supply of suitable high-quality natural diamond specimens, and to the Diamond Trading Company (DTC Research Centre, Maidenhead) for providing and cutting standards and polishing specimens. A.E. Fallick (SURRC) and S.R. Boyd (presently of Université de Nancy) are thanked for combustion mass spectrometer analyses of the standards. We would like to thank: I.L. Chinn (Cape Town University), P. Deines (Pennsylvania State University), J.J. Gurney (Cape Town University), R. Hipkin (University of Edinburgh), P. Kinny (Curtin University, Perth), A. Mainwood (King's College, London), C.M. Welbourn (Diamond Trading Company, Maidenhead), I. Sunagawa (Institute of Gemmology and Jewelry Arts, Yamanashi), W.R. Taylor (Australian National University, Canberra), and R. Thompson (University of Edinburgh) for many useful discussions and helping us to try and understand aspects of the properties of diamonds and statistical distributions. Extremely helpful reviews were also received from A. G. Christie and W.R. Taylor of Australian National University. Despite all this help we remain responsible for any errors in

content or interpretation. The studies were carried out under NERC grants GR3/8562, GR3/5677 and GR3/7479.

References

- Boyd, F.R. and Gurney, J.J. (1986) Diamonds and the African lithosphere. *Science*, **232**, 472–7.
- Boyd, S.R. and Pillinger, C.T. (1994) A preliminary study of $^{15}\text{N}/^{14}\text{N}$ in octahedral growth form diamonds. *Chem. Geol.*, **116**, 43–59.
- Boyd, S.R., Pillinger, C.T., Milledge, H.J., Mendelsohn, M.J. and Seal, M. (1992) C and N isotopic composition and the infrared absorption spectra of coated diamonds: evidence for the regional uniformity of $\text{CO}_2\text{--H}_2\text{O}$ fluids in lithospheric mantle. *Earth Planet. Sci. Lett.*, **109**, 633–44.
- Boyd, S.R., Pineau, F. and Javoy, M. (1994) Modelling the growth of natural diamonds. *Chem. Geol.*, **116**, 29–42.
- Burgess, R., Turner, G., Laurenzi, M., and Harris, J.W. (1989) $^{40}\text{Ar}\text{--}^{39}\text{Ar}$ laser probe dating of individual clinoproxene inclusions in premier eclogitic diamonds. *Earth Planet. Sci. Lett.*, **94**, 22–8.
- Bulanova, G.P. (1995) Origin of Diamond. *J. Geochem. Expl.*, **53**, 1–23.
- Burns, R.C. and Davies, G.J. (1992) Growth of synthetic diamond. In *The properties of natural and synthetic diamond* (J.E. Field, ed.). Academic Press, London, pp. 395–422.
- Burns, R.C., Cvetkovic, V., Dodge, C.N., Evans, D.J.F., Rooney, M.L.T., Spear, P.M. and Welbourn, C.M. (1990) Growth sector dependence of optical features in large synthetic diamonds. *J. Cryst. Growth*, **104**, 257–79.
- Chrenko, R.M., Tuft, R.E. and Strong, H.M. (1977) Transformation of the state of nitrogen in diamond. *Nature*, **270**, 141–4.
- Clark, C.D., Collins, A.T. and Woods, G.S. (1992) Absorption and luminescence spectroscopy. In *The properties of natural and synthetic diamond* (J.E. Field, ed.). Academic Press, London, pp. 35–79.
- Davies, G. (1974) Vibronic spectra in diamond. *J. Physics C: Solid State Physics*, **7**, 3797–809.
- Deines, P. (1980) The carbon isotopic composition of diamonds: relationship to diamond shape, color, occurrence and vapor composition. *Geochim. Cosmochim. Acta*, **44**, 943–61.
- Deines, P. (1996) The role of mantle fluids in the growth of diamonds. In *Advanced materials '96*. Proceedings of 3rd NIRIM Int. Symp. on Advanced Materials (ISAM '96). NIRIM, Tsukuba, pp. 61–4.
- Deines, P., Harris, J.W. and Gurney, J.J. (1991) The carbon isotopic composition and nitrogen content of lithospheric and asthenospheric diamonds from the Jagersfontein and Koffiefontein kimberlite, South Africa. *Geochim. Cosmochim. Acta*, **55**, 2615–25.
- Deines, P., Harris, J.W. and Gurney, J.J. (1993) Depth-related carbon isotope and nitrogen concentration variability in the mantle below the Orapa kimberlite, Botswana, Africa. *Geochim. Cosmochim. Acta*, **57**, 2781–97.
- Dodson, M.H. (1986) Closure profiles in cooling systems. *Mat. Sci. Forum*, **7**, 145–54.
- Eiler, J.M., Valley, J.W., Graham, C.M. and Baumgartner, L.P. (1995) Ion microprobe evidence for the mechanisms of stable isotope retrogression in high-grade metamorphic rocks. *Contrib. Mineral. Petrol.*, **118**, 365–78.
- Evans, T. (1992) Aggregation of nitrogen in diamond. In *The properties of natural and synthetic diamond* (J.E. Field, ed.). Academic Press, London, pp. 259–90.
- Evans, T. and Harris, J.W. (1989) Nitrogen aggregation, inclusion equilibration temperatures and the age of diamonds. In: *Kimberlites and related rocks, vol. 2, The mantle/crustal setting diamonds and diamond exploration* (J. Ross, ed.). Geologic Society of Australia Special Publication, **14**, Blackwell Scientific, Melbourne, pp. 1001–6.
- Field, J.E. (1992) *The properties of natural and synthetic diamond*. Academic Press, London, 710 pp.
- Fitzsimons, I.C.W., Harte, B., Chinn, I.L., Gurney, J.J. and Taylor, W.R. (1999) Extreme chemical variation in complex diamonds from George Creek, Colorado: a SIMS study of nitrogen abundance and carbon isotope composition. *Mineral. Mag.*, **63**, 857–78.
- Fitzsimons, I.C.W., Harte, B. and Clark, R.M. (2000) SIMS stable isotope measurement: counting statistics and analytical precision. *Mineral. Mag.*, in press.
- Galimov, E.M. (1991) Isotope fractionation related to kimberlite magmatism and diamond formation. *Geochim. Cosmochim. Acta*, **55**, 1697–708.
- Gurney, J.J. (1989) Diamonds. In: *Kimberlites and related rocks, vol. 2, The mantle/crustal setting diamonds and diamond exploration* (J. Ross, ed.). Geologic Society of Australia Special Publication, **14**, Blackwell Scientific, Melbourne, pp. 935–65.
- Haggerty, S.E. (1986) Diamond genesis in a multiply-constrained model. *Nature*, **320**, 34–8.
- Harris, J.W. (1987) Recent physical, chemical, and isotopic research of diamond. In *Mantle xenoliths* (P.H. Nixon, ed.). John Wiley & Sons, Chichester, pp. 477–500.
- Harris, J.W. (1992) Diamond geology. In *The properties of natural and synthetic diamond* (J.E. Field, ed.). Academic Press, London, pp. 345–93.
- Harris, J.W. and Gurney, J.J. (1979) Inclusions in diamond. In: *The properties of diamond* (J.E. Field,

- ed.). Academic Press, London, pp. 555–91.
- Harris, J.W., Hawthorne, J.B., Oosterveld, M.M. and Wehmeyer, E. (1975) A classification scheme for diamond and a comparative study of South African diamond characteristics. In: *Physics and Chemistry of the Earth*, 9 (L.H. Ahrens *et al.*, eds). Pergamon, Oxford, pp. 765–83.
- Harte, B. and Otter, M. (1992) Carbon isotope measurements on diamonds. *Chem. Geol.*, **101**, 177–83.
- Hoppe, P., Amari, S., Zinner, E. and Lewis, R.S. (1995) Isotopic compositions of C, N, O, Mg, and Si, trace element abundances, and morphologies of single circumstellar graphite grains in 4 density fractions from the Murchison meteorite. *Geochim. Cosmochim. Acta*, **59**, 4029–56.
- Javoy, M., Pineau, F. and Delorme, H. (1986) Carbon and nitrogen isotopes in the mantle. *Chem. Geol.*, **57**, 41–62.
- Kanda, H. (1996) Temperature effect on impurities in high pressure synthetic diamonds. In *Advanced materials '96*. Proceedings of 3rd NIRIM Int. Symp. Advanced Materials (ISAM '96). NIRIM, Tsukuba, pp. 113–8.
- Kanda, H., Ohsawa, T. and Yamaoka, S. (1990) Formation of nitrogen pairs in synthetic diamond during growth. In *Science and technology of new diamond* (S. Saito *et al.*, eds). Terra Scientific Publishing, Tokyo, pp. 339–44.
- Kirkley, M.B., Gurney, J.J., Otter, M.L., Hill, S.J. and Daniel, L.R. (1991) The application of C isotope measurements to the identification of the sources of C in diamonds: a review. *Appl. Geochem.*, **6**, 477–94.
- Lang, A.R. (1974a) On the growth–sectorial dependence of defects in natural diamonds. *Proc. Roy. Soc. Lond.*, **A340**, 233–48.
- Lang, A.R. (1974b) Space-filling by branching columnar single-crystal growth: an example from crystallisation of diamond. *J. Cryst. Growth*, **23**, 151–3.
- Lang, A.R., Moore, M. and Walmsley, J.C. (1992) Diffraction and imaging studies of diamond. In: *The properties of natural and synthetic diamond* (J.E. Field, ed.). Academic Press, London, pp. 215–58.
- Mainwood, A. (1994) Nitrogen and nitrogen-vacancy complexes and their formation in diamond. *Phys. Rev.*, **B49**, 7934–40.
- Marfunin, A.S. (1979) *Spectroscopy, Luminescence, and Radiation Centers in Minerals*. Translated from the Russian publication by V.V. Schiffer. Springer Verlag, Berlin.
- Marshall, D.J. (1988) *Cathodoluminescence of Geologic Materials*. Unwin Hyman, London.
- McKeegan, K.D., Walker, R.M. and Zinner, E. (1985) Ion microprobe isotopic measurements of individual interplanetary dust particles. *Geochim. Cosmochim. Acta*, **49**, 1971–87.
- Meyer, H.O.A. (1987) Inclusions in diamond. In *Mantle Xenoliths* (P.H. Nixon, ed.). J. Wiley & Sons, Chichester, pp. 501–22.
- Narducci, D. and Cuomo, J.J. (1990) Boron diffusivity in nonimplanted diamond single crystals measured by impedance spectroscopy. *J. Appl. Phys.*, **68**, 1184–6.
- Poferl, D.J., Gardner, N.C. and Angus, J.C. (1973) Growth of boron-doped diamond seed crystals by vapour deposition. *J. Appl. Phys.*, **44**, 1428–34.
- Richardson, S.H. and Harris, J.W. (1997) Antiquity of peridotitic diamonds from the Siberian craton. *Earth Planet. Sci. Lett.* **151**, 271–7.
- Richardson, S.H., Gurney, J.J., Erlank, A.J. and Harris, J.W. (1984) Origin of diamonds in old enriched mantle. *Nature*, **310**, 198–202.
- Richardson, S.H., Harris, J.W. and Gurney, J.J. (1993) Three generations of diamonds from old continental mantle. *Nature*, **366**, 256–8.
- Rickard, R.S., Harris, J.W., Gurney, J.J. and Cardoso, P. (1989) Mineral inclusions in diamonds from the koffiefontein mine. In *Kimberlites and Related Rocks, Vol. 2, the Mantle/Crustal Setting Diamonds and Diamond Exploration* (J. Ross, ed.). Geologic Society of Australia Special Publication, **14**, Blackwell Scientific, Melbourne, pp. 1054–62.
- Robinson, D.N. (1978) The characteristics of natural diamond and their interpretation. *Mineral. Sci. Eng.*, **10**, 55–72.
- Ryan, B.F. and Joiner, B.L. (1994) *Minitab Handbook*. Duxbury Press, Belmont.
- Sato, Y. and Kamo, M. (1992) Synthesis of diamond from the vapour phase. *The Properties of Natural and Synthetic Diamond* (J.E. Field, ed.). Academic Press, London, pp. 423–69.
- Satoh, S., Sumiya, H., Tsuji, K. and Yazu, S. (1990) Difference in nitrogen concentration and aggregation among (111) and (100) growth sectors of large synthetic diamonds. In *Science and technology of new diamond* (S. Saito *et al.*, eds). Terra Scientific Publishing, Tokyo, pp. 351–5.
- Slodzian, G. (1980) Microanalyzers using secondary ion emission. *Adv. Electronics Electron Phys. Suppl.*, **13B**, 1–44.
- Slodzian, G., Wu, T.D., Dennebouy, R., Chaintreau, M., and Rasser, B. (1997) On precision and reproducibility of in situ isotopic measurements. In *Secondary Ion Mass Spectrometry: SIMS X* (A. Benninghoven, B. Hagenhoff and H.W. Werner, eds). John Wiley & Sons, Chichester, pp. 31–38.
- Smith, C.B., Gurney J.J., Harris, J.W., Otter, M.L., Kirkley, M.B. and Jagoutz, E. (1991) Neodymium and strontium isotope systematics of eclogite and websterite paragenesis inclusions from single diamonds, Finsch and Kimberley Pool, RSA. *Geochim.*

- Cosmochim. Acta*, **55**, 2579–90.
- Stoneham, A.M. (1992) Diamond: recent advances in theory. In: *The Properties of Natural and Synthetic Diamond* (J.E. Field, ed.). Academic Press, London, pp. 3–34.
- Sunagawa, I. (1984) Morphology of natural and synthetic diamond crystals. In *Materials science of the Earth's interior* (I. Sunagawa, ed.). Terra Scientific Publishing, Tokyo, pp. 303–30.
- Storms, H.A., Brown, K.F. and Stein J.D. (1977) Evaluation of a cesium positive ion source for secondary ion mass spectrometry. *Anal. Chem.*, **49**, 2023–30.
- Swalin, R.A. (1961) Theoretical calculations of the enthalpies and entropies of diffusion and vacancy formation in semiconductors. *J. Phys. Chem. Solids*, **18**, 290–96.
- Swart, P.K., Pillinger, C.T., Milledge, H.J. and Seal, M. (1983) Carbon isotopic variation within individual diamonds. *Nature*, **303**, 793–5.
- Taylor, W.R., Jaques, A.L. and Ridd, M. (1990) Nitrogen-defect aggregation characteristics of some Australasian diamonds: time-temperature constraints on the source regions of pipe and alluvial diamonds. *Amer. Mineral.*, **75**, 1290–310.
- Taylor, W.R., Canil, D. and Milledge, H.J. (1996) Kinetics of Ib to IaA nitrogen aggregation in diamond. *Geochim. Cosmochim. Acta*, **60**, 4725–33.
- Valley, J.W., Graham, C.M., Harte, B., Eiler, J.M. and Kinny, P.D. (1991) Ion microprobe analysis of oxygen, carbon and hydrogen isotope ratios. In *Application of microanalytical techniques to understanding mineralizing processes* (M.A. McKibben and W.C. Shanks, eds). Reviews in Economic Geology, **7**, pp. 73–98.
- Vavilov, V.S. (1978) Ion implantation into diamond. *Radiat. Eff.*, **37**, 229–36.
- Wentorf, R.H. Jr. and Bovenkerk, H.P. (1962) Preparation of semiconducting diamonds. *J. Chem. Phys.*, **36**, 1987–90.
- Wilding, M.C. (1990) *A study of diamonds with syngenetic inclusions*. Unpubl. Ph.D. thesis, Univ. Edinburgh, 280 pp.
- Wilding, M.C., Harte, B., Fallick, A.E. and Harris, J.W. (1994) Inclusion chemistry, carbon isotopes and nitrogen distribution in diamonds from the Bultfontein mine, South Africa. In: *Proc. 5th Int. Kimberlite Conference* (H.O.A. Meyer and O.H. Leonardos, eds). CPRM Special Publication I/B Jan/94, Brasilia, pp. 116–26.
- Zinner, E., Ming, T. and Anders, E. (1989) Interstellar SiC in the Murchison and Murray meteorites: isotopic composition of Ne, Xe, Si, C and N. *Geochim. Cosmochim. Acta*, **53**, 3273–90.

[Manuscript received 5 January 1998:
revised 30 March 1999]

Plate Captions

PLATE 1. Photograph of the polished 'wild-one' diamond plate (0.4 mm thick plate cut across centre of Bultfontein specimen J/1064.2). This colour photo shows the whole of the plate, with the major discontinuity representing a fracture across the plate; whilst Fig. 2*a* shows the upper part of the specimen on the side analysed, which is the opposite side of the diamond plate to that seen in above. The major zone labels (A, B, C, D, E) correspond with those of Fig. 2*a*, and comparison with Fig. 2*a* shows that although the same broad pattern of zones and subzones is seen on both sides of the diamond plate, there are definite differences in detail. The CL reveals spectacular growth zones of both cuboid and octahedral type. The areas with brighter, lighter blue colours have high N abundances; the very dark and yellow-green coloured subzones (labelled subzones C3, D3, E2 in Fig. 2*a*) are marked by low N abundances. The width of the plate is 3.3 mm.

PLATE 2. (a) Photograph of cut, polished and analysed surface of 'whopper' diamond (off-centre section of Bultfontein specimen J/1063.1) in CL. The interior of the diamond is dominated by a series of largely cuboid growth zones mainly showing high luminescence; whilst the external parts show more regular and planar octahedral growth zones. A narrow zone of virtually zero luminescence is seen as the discontinuous black zone (labelled zone B in Fig. 3) in the outer part of the dominantly cuboid area. The width of the polished section is 4.7 mm. (b) Photograph of cut, polished and analysed surface of Koffiefontein K3 diamond in CL; note that extensive regions at bottom and right of photograph are the rough sides of the diamond, with the margin of the polished surface being marked by a zone (D in Fig. 5) of thin growth lines of variable CL. This diamond shows 'seeds' of rectilinear (octahedral) shape, towards right side of polished surface and marked by dominantly pale/bright blue CL colours. The 'seeds' may join outside the plane of the section and are surrounded by a zone (C of Fig. 5) of fairly uniform dark CL. The maximum width of the polished surface is 2.3 mm.

PLATE 3. Cathodoluminescence photographs of George Creek diamond plates. In all cases the dominant features are illustrated more clearly in the schematic diagrams of Fig. 4. (a) Plate GC008. The surface of this composite diamond comprises a central region with homogeneous buff CL, and outer areas dominated by dark green CL, with bright blue CL growth zones and yellow-green slip planes. The CL features around the dark mineral inclusions are largely obscured by bright patches produced by curving cracks beneath the plate surface. Plate dimensions are 5 mm × 4 mm, and linear trails of SIMS sputter pits are just visible crossing the plate surface. (b) Plate GC030. This composite diamond comprises a central region with yellow CL, and outer areas with blue-green CL and a complex growth zonation. Plate dimensions are 4 mm × 2 mm, and SIMS sputter pits are clearly visible on the plate surface. (c) Plate GC042. This diamond has blue-green CL, and is cut by thin yellowish slip planes in three principal orientations. Plate dimensions are 3 mm × 2 mm, and SIMS sputter pits are clearly visible on the plate surface crossing areas of blue and green CL.

